Inorg. Chem. **2003**, *42*, 8038–8052

Study of Ruthenium(II) Complexes with Anticancer Drugs as Ligands. Design of Metal-Based Phototherapeutic Agents

Renzo Cini,*,† Gabriella Tamasi,† Sandra Defazio,† Maddalena Corsini,‡ Piero Zanello,‡ Luigi Messori,§ Giordana Marcon,§ Francesca Piccioli,§ and Pierluigi Orioli§

Department of Chemical and Biosystem Sciences and Technologies and Department of Chemistry, University of Siena, Via A. Moro 2, I-53100 Siena, Italy, and Department of Chemistry, University of Florence, Via della Lastruccia 3, I-50019 Sesto Fiorentino, Florence, Italy

Received July 31, 2003

The reaction of *trans*-[$RuCl_2(PPh_3)_3$] (Ph = C_6H_5) with 2-thio-1,3-pyrimidine (HTPYM) and 6-thiopurines (TPs) produced mainly crystalline solids that consist of *cis*,*cis*,*trans*-[$Ru(PPh_3)_2(N,S\text{-TPYM})_2$] (**1**) and *cis*,*cis*,*trans*-[$Ru(PPh_3)_2(N^7,S\text{-TPs})_2]X_2$ (X = Cl^-, $CF_3SO_3^-$). In the case of TPs, other coordination isomers have never been isolated and reported. Instead, the mother liquor obtained after filtration of **1** produced red single crystals of *trans*,*cis*,*cis*-[$Ru(PPh_3)_2(N,S\text{-TPYM})_2]\cdot 2H_3O^+\cdot 2Cl^-$ (**2**·$2H_3O^+$·$2Cl^-$). Selected ruthenium(II)–thiobase complexes were studied for their structural, reactivity, spectroscopic, redox, and cytotoxic properties. Single crystals of **1** contain thiopyrimidinato anions chelated to the metal center via N and S. The Ru–N bonds are significantly elongated for **1** [2.122(2) and 2.167(2) Å] with respect to **2** [2.063(3) Å] because of the trans influence from PPh_3. The coordination pseudo-octahedron for **2** is significantly elongated at the apical sites (PPh_3 ligands). Solutions of cis,cis,trans isomers in air are stable for weeks, whereas those of **2** turn green within 24 h, in agreement with the respective redox potentials. *cis*,*cis*,*trans*- and *trans*,*cis*,*cis*-[$Ru(PH_3)_2(N,S\text{-TPYM})_2$], as optimized through the DFT methods at the Becke3LYP level are in good agreement with experimental geometrical parameters (**1** and **2**), with cis,cis,trans being more stable than trans,cis,cis by 3.88 kcal. The trend is confirmed by molecular modeling based on semiempirical (ZINDO/1) and molecular mechanics (MM) methods. Cytotoxic activity measurements for *cis*,*cis*,*trans*-[$Ru(PPh_3)(N\text{-THZ})(N^7,S\text{-}H_2TP)_2]Cl_2$ (**4**) (THZ = thiazole, H_2TP = 6-thiopurine) and *cis*,*cis*,*trans*-[$Ru(PPh_3)_2(N^7,S\text{-HTPR})2]Cl_2$ (**5**) (HTPR = 6-thiopurine riboside) against ovarian cancer cells A2780/S gave IC_{50} values of 17 ± 1 and 29 ± 9 μM, respectively. Furthermore, the spectral analysis of HTPYM, TPs, and their Ru(II) complexes in solution shows that intense absorptions occur in the UVA/vis region of light, whereas standard nucleobases absorb in the UVB region.

Introduction

It has been well established for several years that Ru(II,III) complexes display interesting anticancer, anti-metastatic properties, and some of these compounds are under intensive preclinical and clinical investigation.[1] On the other hand, it is known that thiopurines (6-thiopurine and 6-thioguanine and some of their derivatives) are currently used as antileukemic and antiviral agents and as treatments against several types of other serious disorders such as Crohn's disease.[2] Thiopyrimidines and their derivatives are also investigated for their antiviral potential, as well as for their interesting photochemical properties that can be brought to the design of photodynamic therapies (PDTs).[3a] In general, PDTs represent a promising approach for the treatment of superficial tumors and nonmalignant diseases such as psoriases.[3b−3f] Furthermore, metal complexes that contain phosphines as ligands have shown promising selective cytotoxic and anticancer properties.[3g,3h] Metal complexes of active drugs as ligands can have important pharmaceutical activities because of several factors. In fact, the field mixing coordination chemistry and medicinal chemistry arose a long time ago[4] and is based on certain principles [4a] that can be summarized as follows: Complexation with the metal

* To whom correspondence should be addressed. E-mail: cini@unisi.it.
† Department of Chemical and Biosystem Sciences and Technologies, University of Siena.
‡ Department of Chemistry, University of Siena.
§ Department of Chemistry, University of Florence.

10.1021/ic0349095 CCC: $25.00
Published on Web 11/07/2003

protects the drug against enzymatic degradations because of the inertness of certain metal−ligand linkages. The metal complex can have better hydrophobicity/hydrofilicity properties than the free ligand and, through this, can improve the transport processes in the tissues. In addition, the metal complex can release the active drug(s) in a specific organ, and its activity can be reinforced by the combination of effects from the ligands and from the metal residue. The application of these principles has already resulted in the design of successful metal-based drugs.[5]

Thiopyrimidines and thiopurines are also interesting from the point of view of pure coordination chemistry because of the variety of donation modes that they have exhibited, at least in the solid state (Scheme 1 for selected thiobases). A search on the Cambridge Crystallographic Data Base CCDB (November 2002 release)[6] displayed ca. 60 structures of metal−thiopyrimidine complexes and ca. 30 metal−thiopurine complexes. The most common coordination modes are the chelating ones through N^1,S^2 (a-VIII) or N^3,S^4 (b-III) (thiopyrimidines) and $N,^7S^6$ (d-VI) (thiopurines).

On the basis of these arguments and as a continuation of the work that some of us carried out on ruthenium complexes with thiopurine derivatives,[7] we recently performed a study devoted to the synthesis, structural characterization, and electrochemical property evaluation, as well as the estimation of selected biological parameters, of ruthenium complexes with thiopurines and thiopyrimidines. We report here on selected results from this study, such as the crystal and molecular structures of two ruthenium−thiopyrimidine complexes; the molecular modeling analysis of selected molecules; and the redox, spectrophotometric, and cytotoxic properties of these molecules.

Experimental Section

Materials. $RuCl_3 \cdot 3H_2O$ and triphenylphosphine (PPh_3) were obtained from Aldrich (Dorset, U.K.). 6-Thiopurine (H_2TP), 6-thiopurine riboside (HTPR), 2-thio-1,3-pyrimidine (HTPYM), were purchased from Sigma (Seelze, Germany). All of the reagents were used as received without any further purification. TLC plates of silica gel and silica gel C18-100 were obtained from Macherey-Nagel GmbH & Co. (Düren, Germany). Bovine serum albumin (BSA), horse serum, RPMI 1640, fetal bovine serum (FBS), streptomycin, penicillin, sulforhodamine B (SRB), and calf thymus DNA were also purchased from Sigma.

trans-$[RuCl_2(PPh_3)_3]$, **3**, was obtained as previously reported by others.[8] *cis*,*cis*,*trans*-$[Ru(PPh_3)(N\text{-THZ})(N^7,S\text{-}H_2TP)_2]Cl_2 \cdot 2H_2O$, **4**·$2H_2O$[7c] and *cis*,*cis*,*trans*-$[Ru(PPh_3)_2(N^7,S\text{-HTPR})_2]Cl_2 \cdot 2.75H_2O$, **5**·$2.75H_2O$[7d] were obtained as previously reported by this laboratory; their purity was checked via ^1H NMR spectroscopy.

Synthesis of *cis*,*cis*,*trans*-[Ru(PPh$_3$)$_2$(*N*,*S*-TPYM)$_2$], 1. Fifty-two milligrams of HTPYM (MW = 112.2, 0.46 mmol) was mixed with absolute EtOH (10 mL), and the resulting suspension was deareated with a stream of ultrapure nitrogen under stirring at 25 °C. Then, 220 mg of **3** (MW = 958.8, 0.23 mmol) was added to the suspension, and the resulting mixture was refluxed under nitrogen. An orange crystalline solid started to precipitate after 10 min of refluxing; heating and stirring were continued for 2 h. The yellow suspension was then cooled to 25 °C and stored for 2 h, and then the solid was filtered off, and the mother liquor was set apart. The orange solid was washed twice with absolute EtOH and twice with Et_2O and was finally dried in a vacuum at 25 °C for 24 h. The crude product was recrystallized from CH_2Cl_2. Yield, 62%. Single crystals (orange) suitable for X-ray diffraction studies were obtained by slowly evaporating saturated CH_2Cl_2 solutions of the purified compound. Anal. Found (Mikroanalytisches Labor Pascher, Remagen, Germany) (%): C, 62.58; H, 4.13; N, 6.37; P, 6.99; S, 7.05. Calcd for $C_{44}H_{36}N_4P_2RuS_2$ (MW = 847.90) (%): C, 62.33; H, 4.28; N, 6.61; P, 7.31; S, 7.56. IR: 1558 cm^{-1} [sh (sharp), m (medium intensity)], 1541 (sh, m), 1366 [sh, s (strong)], 1183 (m),

(1) (a) Akbayeva, D.; Gonsalvi, L.; Oberhauser, W.; Peruzzini, M.; Vizza, F.; Brugeller, P.; Romerosa, A.; Sava, G.; Bergamo, A. *Chem. Commun.* **2003**, 264. (b) Pintus, G.; Tadolini, B.; Posadino, A. M.; Sanna, B.; Debidda, M.; Bennardini, F.; Sava, G.; Ventura, C. *Eur. J. Biochem.* **2002**, *269*, 5861. (c) Frausin, F.; Cocchietto, M.; Bergamo, A.; Scarcia, V.; Furlani, A.; Sava, G. *Cancer Chemother. Pharmacol.* **2002**, *50*, 405. (d) Zorzet, S.; Bergamo, A.; Cocchietto, M.; Sorc, A.; Gava, B.; Alessio, E.; Iengo, E.; Sava, G. *J. Pharmacol. Expl. Ther.* **2000**, *295*, 927. (e) Morris, R. E.; Aird, R. E.; del Socorro Murdoch, P.; Chen, H.; Cummings, J.; Hughes, N. D.; Parsons, S.; Parkin, A.; Boyd, G.; Jodrell, D. I.; Sadler, P. J. *J. Med. Chem.* **2001**, *44*, 3616. (f) Wang, F.; Chen, H.; Parkinson, J. A.; del Socorro Murdoch, P.; Sadler, P. J. *Inorg. Chem.* **2002**, *41*, 4509. (g) Chen, H.; Parkinson, J. A.; Parsons, S.; Coxall, R. A.; Gould, R. O.; Sadler, P. J. *J. Am. Chem. Soc.* **2002**, *124*, 3064. (h) Gallori, E.; Vettori, C.; Alessio, E.; Gonzalez Vilchez, F.; Vilaplana, R.; Orioli, P.; Casini, A.; Messori, L. *Arch. Biochem. Biophys.* **2000**, *376*, 156. (i) Küng, A.; Pieper, T.; Keppler, B. K. *J. Chromatogr. B: Biomed. Sci. Appl.* **2001**, *759*, 81. (j) Abufarag, A.; Reedijk, J. *J. Inorg. Biochem.* **1995**, *59*, 137. (k) Dhubhghaill, O. M. N.; Hagen, W. R.; Keppler, B. K.; Lipponer, K.-G.; Sadler, P. J. *J. Chem. Soc., Dalton Trans.* **1994**, 3305. (l) Hartmann, M.; Lipponer, K.-G.; Keppler, B. K. *Inorg. Chim. Acta* **1998**, *267*, 137. (m) Clarke, M. J.; Zhu, F.; Frasca, D. *Chem. Rev.* **1999**, *99*, 2511. (n) Frasca, D.; Clarke, M. J. *J. Am. Chem. Soc.* **1999**, *121*, 8523.

(2) (a) Nielsen, O. H.; Vainer, B.; Rask-Madsen, J. *Aliment. Pharmacol. Ther.* **2001**, *15*, 1699. (b) De Abreu, R. A.; Bokkerink, J. P.; Keuzenkamp-Jansen, C. W.; Stet, E. H.; Trijbels, J. F. *Adv. Exp. Med. Biol.* **1998**, *431*, 687. (c) Markowitz, J. F. *Rev. Gastroenterol. Disord.* **2003**, 3 Suppl 1, S23. (d) Nielsen, O. H.; Vainer, B.; Rask-Madsen J. *Aliment. Pharmacol. Ther.* **2001**, *15*, 1699. (e) Dubinsky, M. C.; Hassard, P. V.; Seidman, E. G.; Kam, L. Y.; Abreu, M. T.; Targan, S. R.; Vasiliauskas, E. A. *Inflamm. Bowel Dis.* **2001**, *7*, 181.

(3) (a) Massey, A.; Xu, Y. Z.; Karran, P. *Curr. Biol.* **2001**, *11*, 1142. (b) Shigeta, S.; Mori, S.; Watanabe, F.; Takahashi, K.; Nagata, T.; Koike, N.; Wakayama, T.; Saneyoshi, M. *Antivir. Chem. Chemother.* **2002**, *13*, 67. (c) Hruza, G. *Health News* **2002**, *8*, 3. (d) Vrouenraets, M. B.; Visser, G. W. M.; Snow, G. B.; van Dongen, G. A. M. S. *Anticancer Res.* **2003**, *23*, 505. (e) Jurklies, B.; Anastassiou, G.; Ortmans, S.; Schuler, A.; Schilling, H.; Schmidt-Erfurth, U.; Bornfeld, N. *Br. J. Ophthalmol.* **2003**, *87*, 84. (f) Schmidt-Erfurth, U. M.; Michels, S.; Kusserow, C.; Jurklies, B.; Augustin, A. *Ophthalmologica* **2002**, *109*, 2284. (g) McKeage, M. J.; Maharaj, L.; Berners-Price, S. J. *Coord. Chem. Rev.* **2002**, *232*, 127. (h) Zhang, J.; Vittal, J. J.; Henderson, W.; Wheaton, J. R.; Hall, I. H.; Hor, T. S. A.; Yan, Y. K. *J. Organomet. Chem.* **2002**, *650*, 123.

(4) (a) Dubler, E. *Metal Ions in Biological Systems*; Sigel, A., Sigel, H., Eds.; Marcel Dekker: New York, 1996; Chapter 8. (b) Farrell, N. P. *Uses of Inorganic Chemistry in Medicine*; The Royal Society of Chemistry: London, 1999.

(5) (a) Weder, J. E.; Hambley, T. W.; Kennedy, B. J.; Lay, P. A.; Foran, G. J.; Rich, A M. *Inorg. Chem.* **2001**, *40*, 1295. (b) Zhou, Q.; Hambley, T. W.; Kennedy, B. J.; Lay, P. A.; Turner, P.; Warwick, B.; Biffin, J. R.; Regtop, H. L. *Inorg. Chem.* **2000**, *39*, 3742. (c) Weder, J. E.; Hambley, T. W.; Kennedy, B. J.; Lay, P. A.; MacLachlan, D.; Bramley, R.; Delfs, C. D.; Murray, K. S.; Moubaraki, B.; Warwick, B.; Biffin, J. R.; Regtop, H. L. *Inorg. Chem.* **1999**, *38*, 1736.

(6) *The Cambridge Crystallographic Data Base*, version 5.24; The Cambridge Crystallographic Data Center: Cambridge, U.K., Nov 2002.

(7) (a) Cini, R.; Bellucci, C.; Tamasi, G.; Corsini, M.; Fontani, M.; Zanello, P. *Inorg. Chim. Acta* **2002**, *339*, 89. (b) Bellucci, C.; Cini, R. *J. Inorg. Biochem.* **1999**, *76*, 243. (c) Pifferi, C.; Cini, R. *J. Chem. Soc., Dalton Trans.* **1998**, 2679. (d) Cini, R.; Bozzi, R.; Karaulov, A.; Hursthouse, M. B.; Calafat, A. M.; Marzilli, L. G. *J. Chem. Soc., Chem. Commun.* **1993**, 899. (e) Cini, R.; Cinquantini, A.; Sabat, M.; Marzilli, L. G. *Inorg. Chem.* **1985**, *24*, 3903.

(8) Stephenson, T. A.; Wilkinson, G. *J. Inorg. Nucl. Chem.* **1966**, *28*, 945.

Scheme 1. Coordination Arrangements for (a) 2-Thio-1,3-pyrimidine, (b) 4-Thio-1,3-pyrimidines, (c) 2,4-Dithio-1,3-pyrimidine(dithiouracyl), and (d) 6-Thiopurines[a]

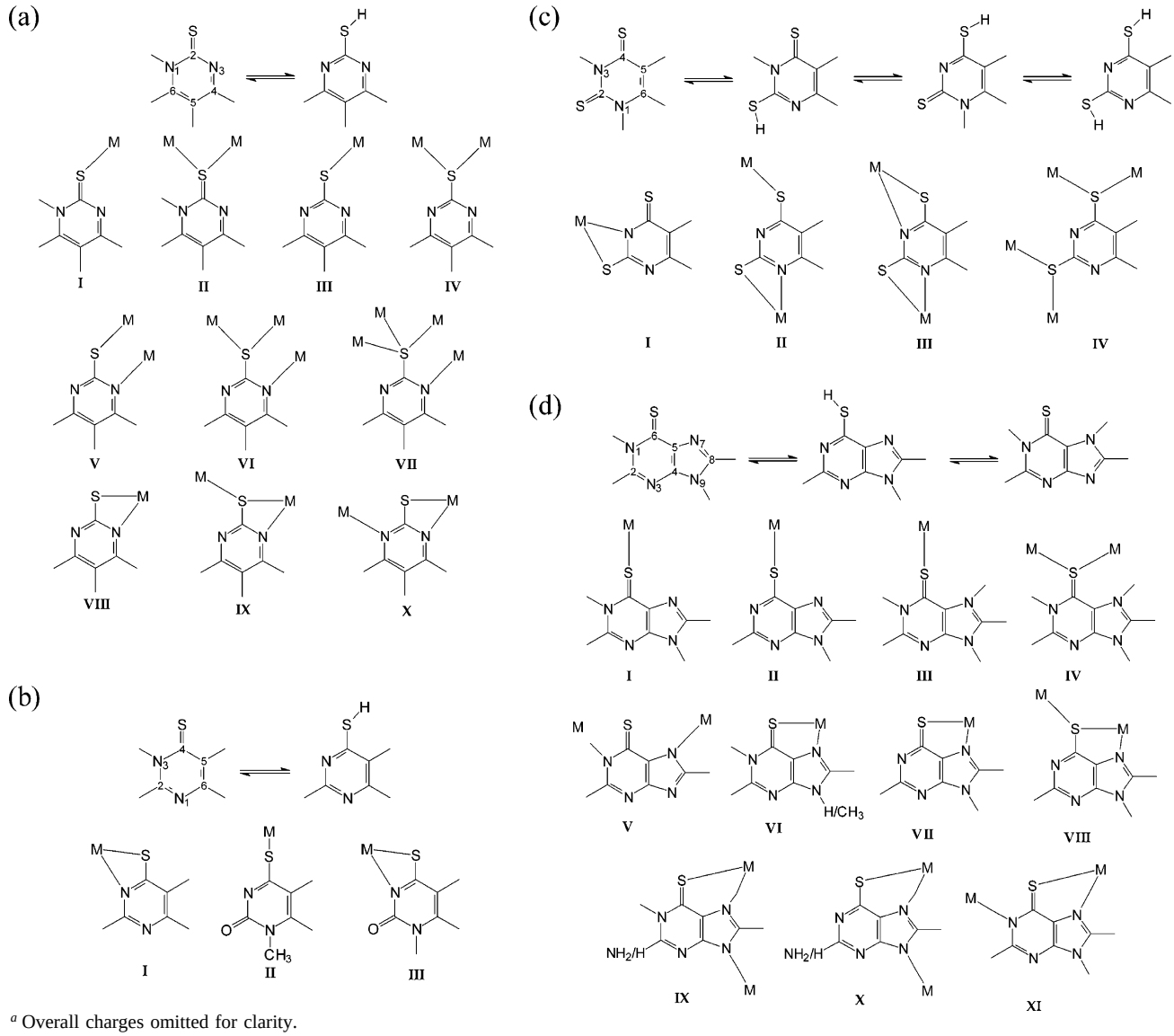

[a] Overall charges omitted for clarity.

746 (m), 696 (sh, s), 519 (sh, s); free HTPYM, 3053 cm^{-1} (sh, m), 1607 (sh, s), 1569 (sh, m), 1332 (sh, s), 1186 (sh, s), 982 (sh, m), 793 (sh, m), 749 (sh, m), 471 (sh, m). UV/vis (CH_2Cl_2): 239 nm (ϵ, 48770 mol^{-1} cm^{-1} L), 330 (13800). UV/vis (DMSO): 328 (20640, broad), ca. 350 (ca. 14200, shoulder); free HTPYM (DMSO): 293 (22700), 371 (2060), 382 (2060). ^1H NMR ($CDCl_3$): 7.92−7.89 ppm from TMS (1H, m = multiplet, H^6), 7.64−7.60 (1H, m, H^4), 7.32−6.97 (15H, m, PPh_3), 6.09−6.04 (1H, t = triplet, H^5). Free HTPYM, not soluble in $CDCl_3$. TLC (C18−100, CH_3CN): Rf, 0.76. TLC (C18−100, CH_3CN 95%, H_2O 5%): 0.80. Single crystals suitable for X-ray diffraction of **1** can be grown also by dissolving the purified complex (20 mg) in dry DMSO (10 mL) at 70 °C and storing the solution at 25 °C in an air atmosphere for several days.

Synthesis of *trans,cis,cis*-[Ru(PPh$_3$)$_2$(*N,S*-TPYM)$_2$]·2H$_3$O$^+$·2Cl$^-$, 2·2H$_3$O$^+$·2Cl$^-$. The mother solution collected from the preparation of **1** (see above) was spontaneously concentrated by slow evaporation in the air atmosphere at 25 °C. Once the solution reached dryness, a small amount of red needle-shaped crystals formed. The crystals were collected with the help of a stainless rod; they appeared to be suitable for X-ray diffraction analysis when examined under a polarizing microscope. Yield, 4%. Anal. Found (EDAX, scanning electron microscopy): Ru/P, 0.52 ± 0.04; Ru/S, 0.46 ± 0.04; Ru/Cl, 0.44 ± 0.06 atom/atom. Calcd for $C_{44}H_{42}Cl_2N_4O_2P_2RuS_2$ (MW = 956.85): Ru/P, 0.50; Ru/S, 0.50; Ru/Cl, 0.50 atom/atom. IR: 3400 cm^{-1} [br (broad), s], 1609 (br, m), 1566 (sh, m), 1547 (sh, m), 1372 (sh, m), 1180 (br, m), 739 (sh, m), 687 (sh, s), 516 (sh, s). UV/vis (CH_2Cl_2, slightly soluble): 325 nm (ϵ, ca. 9000 mol^{-1} cm^{-1} L); after 1 day from mixing, the solution is green, and a band at 590 nm (ϵ, ca. 259 mol^{-1} cm^{-1} L) appears. ^1H NMR ($CDCl_3$): 7.97−7.94 ppm from TMS (1H, m, H^6), 7.54−7.60 (1H, m, H^4), 7.35−7.05 (15H, m, PPh_3), 6.19−6.16 (1H, t, H^5). TLC (C18−100, CH_3CN): Rf, 0.86. TLC (C18−100, CH_3CN 95%, H_2O 5%): 0.89.

X-ray Crystallography. Well-formed orange parallelepiped and red needle-shaped crystals of **1** and **2**·2H_3O^+·2Cl^-, respectively, were selected under the polarizing microscope, mounted on glass capillaries, and then subjected to diffraction experiments through a Siemens P4 automatic four-circle diffractometer at 293 ± 2 K. Accurate cell constant measurements (Table 1) were performed by using full-matrix least-squares refinement of the values of 25 and 30 carefully centered randomly selected reflections in the ranges $10 \le 2\theta \le 48°$ and $14 \le 2\theta \le 36°$ for the two compounds, respectively. The diffraction data sets (7740 and 4708 reflections)

Table 1. Selected Crystal Data and Structure Refinement Data for *cis*,*cis*,*trans*-[$Ru(PPh_3)_2(N,S\text{-TPYM})_2$] (**1**) and *trans*,*cis*,*cis*-[$Ru(PPh_3)_2(N,S\text{-TPYM})_2$]·$2H_3O^+$·$2Cl^-$ (**2**·$2H_3O^+$·$2Cl^-$)

parameter	value	
	1	**2**·$2H_3O^+$·$2Cl^-$
empirical formula	$C_{44}H_{36}N_4P_2RuS_2$	$C_{44}H_{42}Cl_2N_4O_2P_2RuS_2$
formula weight	847.90	956.85
temperature (K)	293(2)	293(2)
wavelength (Å)	0.71073	0.71073
crystal system	triclinic	monoclinic
space group	*P*-1 (no. 2)	*C*2/*c* (no. 15)
unit cell dimensions		
a (Å)	11.188(3)	15.728(1)
b (Å)	13.194(3)	12.974(1)
c (Å)	14.853(4)	21.923(5)
α (°)	77.04(2)	90
β (°)	71.39(2)	103.41(1)
γ (°)	66.41(2)	90
volume ($Å^3$)	1892.4(8)	4351.5(11)
Z	2	4
calculated density (Mg/m^3)	1.488	1.461
absorption coefficient (mm^{-1})	0.648	0.695
refinement method	full-matrix least-squares on F^2	full-matrix least-squares on F^2
data/restraints/parameters	6636/0/478	3834/0/258
GOF on F^2	0.969	0.818
final *R* indices [$I > 2\sigma(I)$]	R1 = 0.0322, wR2 = 0.0851	R1 = 0.0357, wR2 = 0.0908
R indices (all data)	R1 = 0.0369, wR2 = 0.0885	R1 = 0.0499, wR2 = 0.1008

were corrected for Lorentz polarization and absorption (*ψ*-scan) effects. The structure solutions and refinements were carried out through the Patterson and Fourier synthesis methods and full-matrix least-squares cycles. The asymmetric unit cell of **1** contains the entire complex molecule, whereas that of **2**·$2H_3O^+$·$2Cl^-$ consists of one-half of a complex molecule, a H_3O^+ cation, and a Cl^- anion. All of the non-hydrogen atoms of **1** and **2** were treated as anisotropic; all of the hydrogen atoms were considered as isotropic. The hydrogen atoms of H_3O^+ for **2**·$2H_3O^+$·$2Cl^-$ were not included at all in the refinement. All calculations were performed using the SHELX97[9] and PARST97[10] packages, whereas the graphics outputs were obtained by using the XPMA-ZORTEP[11] and ORTEP32[12] computer programs implemented on PC Pentium IV machines.

Spectroscopy. IR. IR spectra were recorded at 25 ± 1 °C from KBr matrix pellets using a Perkin-Elmer model 1600 FT-IR spectrometer.

UV/vis. UV/vis spectra were recorded at 25 ± 1 °C from solutions contained in 1-cm-path-length quartz cuvettes using a Perkin-Elmer EZ-201 spectrophotometer. Visible absorption spectra for the biological experiments were carried out at 25 °C using a Perkin-Elmer Lambda Bio 20 instrument.

^{1}H NMR. ^{1}H NMR spectra were obtained at 22 ± 1 °C through Varian XL-200 and Bruker DRX-600 spectrometers working at 200 and 600 MHz, respectively. The concentration of each sample was 1×10^{-2} M.

Electrochemistry. Materials and apparatus for electrochemistry have been described elsewhere.[13] All potential values are referred to the saturated calomel electrode (SCE). Under the present experimental conditions, the one-electron oxidation of ferrocene occurs at +0.39 V in CH_2Cl_2 solution and +0.38 V in DMSO solution.

Ultrafiltration Experiments. The adducts between Ru(II)-complexes and the biological target (BSA and calf thymus DNA) were filtered after a 24-h incubation at room temperature using a Centricon YM-10 device (10000 Da, Amicon Bioseparations, Millipore Corporation, Billerica, MA), and the starting volume was reduced to one-half. Finally, the absorption spectra of the upper and lower portions of the solution were recorded. Where not differently stated, experiments were performed in phosphate buffer containing NaH_2PO_4 (50 mM) and NaCl (100 mM), pH 7.4.

Cell Culture and Cytotoxicity Assay. In vitro cytotoxicity assays on cultured human tumor cell lines still represent the standard method for the initial screening of antitumor agents. The disease-oriented primary screen of the NCI is based on a panel of 60 different tumor cell lines. Thus, as a first step for their pharmacological evaluation, the Ru(II) complexes were assayed toward a restricted panel of tumor cell lines. This panel comprised two ovarian carcinoma A2780 (both sensitive, S, and resistant, R, to cisplatin) human cell lines; the colon carcinoma HT29 cell line; the breast carcinoma MCF7 cell line; and finally, the lung carcinoma A549 cell line. The cisplatin-resistant A2780/R cell line was produced by repeated 1-h weekly exposures to 50 mM solutions of the sensitive parental cell line.[14] Cell lines were cultured in RPMI 1640 medium supplemented with 10% horse serum (HT29, MCF7, and A549) or FBS (A2780/S and A2780/R) and antibiotics (streptomycin 100 mg/mL and penicillin 100 U/mL) at 37 °C in a 5% CO_2 atm and subcultured twice weekly. Experiments were conducted on exponentially growing cells. Drugs were dissolved in sterile DMSO. Inhibition of cell growth was determined after a 72-h drug exposure by the SRB assay performed in 96-well plates, using RPMI 1640 medium plus 5% FBS, according to the protocol of Skehan.[15]

Molecular Modeling Methods. Density Functional. All density functional calculations were performed with the Gaussian 98

(9) (a) Sheldrick, G. M. *SHELXS 97, Program for the Solution of Crystal Structures*; University of Göttingen: Göttingen, Germany, 1997. (b) Sheldrick, G. M. *SHELXL 97, Program for the Refinement of Crystal Structures*; University of Göttingen: Göttingen, Germany, 1997.
(10) Nardelli, M. *PARST 97, A System of Computer Routines for Calculating Molecular Parameters from Results of Crystal Structure Analyses*; University of Parma: Parma, Italy, 1997.
(11) Zsolnai, L. *XPMA-ZORTEP-98*; University of Heidelberg: Heidelberg, Germany, 1996.
(12) Johnson, C. K.; Burnett, M. N. *ORTEP-3 for Windows*; Oak Ridge National Laboratory: Oak Ridge, TN. 32-bit Implementation by Farrugia, L. J. University of Glasgow, Glasgow, Scotland, 1998.
(13) Fabrizi de Biani, A. F.; Laschi, F.; Zanello, P.; Ferguson, G.; Trotter, J.; O'Riordan, G. M.; Spalding, T. R. *J. Chem. Soc., Dalton Trans.* **2001**, 1520.
(14) Lu, Y.; Han, J.; Scanlon, K. J. *J. Biol. Chem.* **1988**, *263*, 4891.
(15) Skehan, P.; Storeng, R.; Scudiero, D.; Monks, A.; McMahon, J.; Vistica, D.; Warren, J. T.; Bokesch, H.; Kenney, S.; Boyd, M. R. *J. Natl. Cancer Inst.* **1990**, *82*, 1107.

Table 2. Selected AMBER-type Force Field Parameters Used to Model *cis*,*cis*,*trans*-, *trans*,*cis*,*cis*-, *trans*,*trans*,*trans*-[Ru(PPh$_3$)$_2$(*N*,*S*-TPYM)$_2$] via MM Methods

vector[a]	r_o (Å)	k_r (kcal Å^{-2} mol^{-1})	vector[a]	r_o (Å)	k_r (kcal Å^{-2} mol^{-1})
Z0*P0	2.35	200.0	Z0*N0	2.05	150.0
Z0*S0	2.40	200.0	P0*C2	1.83	419.0

vectors[a]	θ (°)	k_θ (kcal rad^{-2} mol^{-1})	vectors[a]	θ (°)	k_θ (kcal rad^{-2} mol^{-1})
P0*Z0*P0	180.0	25.0 (tcc, ttt)	S0*Z0*N0	90.0	15.0 (tcc, ttt)
	90.0	15.0 (cct)		180.0	25.0 (cct)
P0*Z0*S0	90.0	15.0	N0*Z0*N0	180.0	25.0 (ttt)
P0*Z0*N0	90.0	15.0		90.0	15.0 (cct, tcc)
S0*Z0*S0	180.0	25.0 (cct, ttt)	Z0*P0*C2	113.0	20.0
	90.0	15.0 (tcc)	C2*P0*C2	93.0	69.0

	charge (e)			charge (e)	
atom	cct	tcc, ttt	atom	cct	tcc, ttt
Ru1	−0.072	0.000	C6	−0.195	−0.192
P1	0.060	0.070	H4	0.246	0.247
S1	0.049	0.063	H5	0.235	0.233
N1	−0.221	−0.241	H6	0.274	0.225
C2	−0.064	−0.085	C(P)(PPh$_3$)	0.000	0.004
N3	0.016	0.020	C(H)(PPh$_3$)	−0.150	−0.150
C4	−0.312	−0.313	H(PPh$_3$)	0.158	0.159
C5	−0.172	−0.174			

[a] * = any bond.

(revision A.7) package[16] implemented on an Origin 3800 SG machine. Geometry optimizations, population analyses, and vibration frequency calculations were obtained using the Becke3LYP method[17] and different basis sets[17] depending on the atom type and on the molecule. The models analyzed were as follows: TPYM$^-$ (MOD-E), *cis*,*cis*,*trans*-[Ru(PH$_3$)$_2$(*N*,*S*-TPYM)$_2$] (MOD-Jcct), and *trans*,*cis*,*cis*-[Ru(PH$_3$)$_2$(*N*,*S*-TPYM)$_2$] (MOD-Jtcc). Molecular drawings were obtained through the ORTEP32[12] package.

Semiempirical. Semiempirical calculations were carried out using the HyperChem 5.1[18] package and the ZINDO/1 level of approximation.[19a] The molecular models investigated were as follows: PH_3 (MOD-A), NH_3 (MOD-A′), H_2S (MOD-A″), HS^- (MOD-A‴), PPh_3 (MOD-B), H(N1)-$C_4H_4N_2S$ (HTPYM, MOD-C), H(N1),H(N9)-$C_5H_4N_4S$ (H_2TP, MOD-C′), H(N1),H(N7)-$C_5H_4N_4S$ (H_2TP, MOD-C″), H(S)-$C_4H_4N_2S$ (HTMPYM, MOD-D), C_3H_4NS (THZ, MOD-D′), TPYM$^-$ (MOD-E), *cis*,*trans*,*cis*-[Ru(NH$_3$)$_2$(PH$_3$)$_2$(H$_2$S)$_2$]$^{2+}$ (MOD-Fctc, Scheme 2), *cis*,*cis*,*trans*-[Ru(NH$_3$)$_2$(PH$_3$)$_2$(H$_2$S)$_2$]$^{2+}$ (MOD-Fcct), *cis*,*trans*,*cis*-[Ru(NH$_3$)$_2$(PH$_3$)$_2$(HS)$_2$] (MOD-Gctc), *cis*,*cis*,*trans*-[Ru(NH$_3$)$_2$(PH$_3$)$_2$(HS)$_2$] (MOD-Gcct), [Ru(*N*,*S*-TPYM)]$^+$ (MOD-H), *cis*,*cis*,*trans*-[Ru(NH$_3$)$_2$(*N*,*S*-TPYM)$_2$] (MOD-Icct), *cis*,*cis*,*cis*-[Ru(PH$_3$)$_2$(*N*,*S*-TPYM)$_2$] (MOD-Jccc), *trans*,*cis*,*cis*-[Ru(PH$_3$)$_2$(*N*,*S*-TPYM)$_2$] (MOD-Jtcc), *cis*,*trans*,*cis*-[Ru(PH$_3$)$_2$(*N*,*S*-TPYM)$_2$] (MOD-Jctc), *cis*,*cis*,*trans*-[Ru(PH$_3$)$_2$(*N*,*S*-TPYM)$_2$] (MOD-Jcct), *trans*,*trans*,*trans*-[Ru(PH$_3$)$_2$(*N*,*S*-TPYM)$_2$] (MOD-Jttt), *cis*,*cis*,*cis*-[Ru(PH$_3$)$_2$(*N*^{7},*S*-H$_2$TP)$_2$]$^{2+}$ (MOD-Kccc), *cis*,*cis*,*trans*-[Ru(PH$_3$)$_2$(*N*^{7},*S*-H$_2$TP)$_2$]$^{2+}$ (MOD-Kcct), *trans*,*trans*,*trans*-[Ru(PH$_3$)$_2$(*N*^{7},*S*-H$_2$TP)$_2$]$^{2+}$ (MOD-Kttt), *cis*,*cis*,*trans*-[Ru(PH$_3$)(*N*-THZ)(*N*^{7},*S*-H$_2$TP)$_2$]$^{2+}$ (MOD-Mcct), and *trans*,*trans*,*trans*-[Ru(PH$_3$)(*N*-THZ)(*N*^{7},*S*-H$_2$TP)$_2$]$^{2+}$ (MOD-Mttt). All molecules were refined to a root-mean square gradient of 0.01 kcal. The analysis of the vibration motions did not show any negative frequency. The UV/vis spectra for the ligand molecules and for MOD-H were computed at the ZINDO/S[19] level on the structures previously fully optimized at ZINDO/1.

Molecular Mechanics (MM). Molecular mechanics calculations and graphical visualizations were performed by using the MacroModel 5.0 package (MMOD)[20] implemented on a Silicon Graphics SG Indigo 2 workstation. The parametrization was based on the Amber force field[21] but was extensively changed to fit the requirements of the specific groupings and coordination-sphere atoms. A trial-and-error procedure was used to finally refine the force field parameters that were based on the data found from the vibration analysis carried out in advance via density functional and molecular orbital methods. The final force fields gave good agreement between the computed and experimental (solid-state) structures (Table 2). The molecules optimized were PPh_3 (MOD-B), HTPYM (MOD-C), TPYM$^-$ (MOD-E), *trans*,*cis*,*cis*-[Ru(PPh$_3$)$_2$(*N*,*S*-TPYM)$_2$] (MOD-Ltcc), *cis*,*cis*,*trans*-[Ru(PPh$_3$)$_2$(*N*,*S*-TPYM)$_2$] (MOD-Lcct), *trans*,*trans*,*trans*-[Ru(PPh$_3$)$_2$(*N*,*S*-TPYM)$_2$] (MOD-Lttt), *cis*,*cis*,*trans*-[Ru(PPh$_3$)(*N*-THZ)(*N*^{7},*S*-H$_2$TP)$_2$]$^{2+}$ (MOD-Ncct), and *trans*,*trans*,*trans*-[Ru(PPh$_3$)(*N*-THZ)(*N*^{7},*S*-H$_2$TP)$_2$]$^{2+}$ (MOD-Nttt). All optimizations were performed to a root-mean square gradient of 0.01 kcal mol^{-1}.

(16) Frisch, M. J.; Trucks, G. W.; Schlegel, H. B.; Scuseria, G. E.; Robb, M. A.; Cheeseman, J. R.; Zakrzewski, V. G.; Montgomery, J. A., Jr.; Stratmann, R. E.; Burant, J. C.; Dapprich, S.; Millam, J. M.; Daniels, A. D.; Kudin, K. N.; Strain, M. C.; Farkas, O.; Tomasi, J.; Barone, V.; Cossi, M.; Cammi, R.; Mennucci, B.; Pomelli, C.; Adamo, C.; Clifford, S.; Ochterski, J.; Petersson, G. A.; Ayala, P. Y.; Cui, Q.; Morokuma, K.; Malick, D. K.; Rabuck, A. D.; Raghavachari, K.; Foresman, J. B.; Cioslowski, J.; Ortiz, J. V.; Baboul, A. G.; Stefanov, B. B.; Liu, G.; Liashenko, A.; Piskorz, P.; Komaromi, I.; Gomperts, R.; Martin, R. L.; Fox, D. J.; Keith, T.; Al-Laham, M. A.; Peng, C. Y.; Nanayakkara, A.; Gonzalez, C.; Challacombe, M.; Gill, P. M. W.; Johnson, B.; Chen, W.; Wong, M. W.; Andres, J. L.; Gonzalez, C.; Head-Gordon, M.; Replogle, E. S.; Pople, J. A. *Gaussian 98*, revision A.7; Gaussian Inc.: Pittsburgh, PA, 1998.

(17) Frisch, A.; Frisch, M. J. *Gaussian 98, User's Reference*, 2nd ed.; Gaussian Inc.: Pittsburgh, PA, 1998.

(18) *HyperChem, Molecular Modeling System*, release 5.1 Pro for Windows; Hypercube Inc.: Gainesville, FL, 1997.

(19) (a) HyperChem, *Reference Manual*; Hypercube Inc.: Gainesville, FL, 1997. (b) The parametrization of ZINDO/S files for the Ru atom was that previously reported: Krogh-Jespersen, K.; Westbrook, J. D.; Potenza, J. A.; Schugar, H. J. *J. Am. Chem. Soc.* **1987**, *109*, 7025. Masui, H.; Freda, A. L.; Zerner, M. C.; Lever, A. B. P. *Inorg. Chem.* **2000**, *39*, 141.

(20) Mohamadi, F.; Richards, N. G. J.; Guida, W. C.; Liskamp, R.; Lipton, M.; Caufield, C.; Chang, G.; Hendrickson, T.; Still, W. C. *J. Comput. Chem.* **1990**, *11*, 440.

(21) Cornell, W. D.; Cieplak, P.; Bayly, C. I.; Gould, I. R.; Merz, K. M., Jr.; Ferguson, D. M.; Spellmeyer, D. C.; Fox, T.; Caldwell J. W.; Kollman, P. A. *J. Am. Chem. Soc.* **1995**, *117*, 5179.

Scheme 2. Selected Molecules Determined via Molecular Modeling Analysis

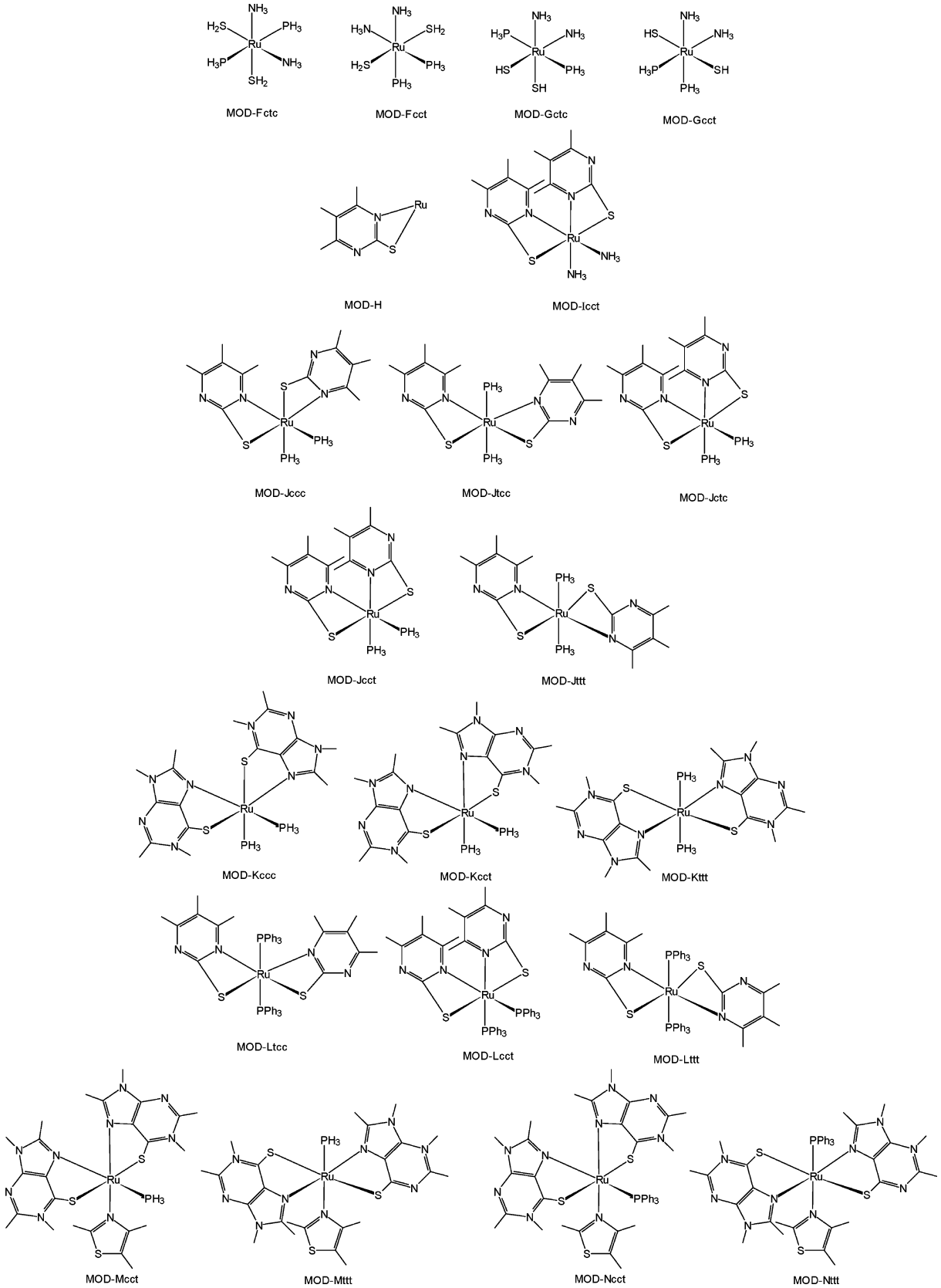

Results and Discussion

Reaction of *trans*-[$RuCl_2(PPh_3)_3$] with Thiobases. *trans*-[$RuCl_2(PPh_3)_3$], **3**, was selected as starting ruthenium compound for investigating reactions with thiobases because (a) it can be easily prepared in high yield from $RuCl_3 \cdot 3H_2O$,[8] (b) it contains a coordinatively and electronically unsaturated Ru(II) center that can predictably be stabilized by Ru−N

Scheme 3. Possible Octahedral Isomers for $[Ru(P)_2(N-S)_2]$ Bischelates

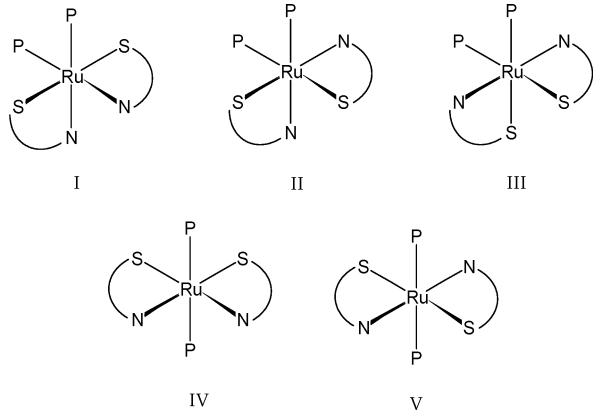

and/or Ru−S linkages with thiobases, and (c) the high trans effect/influence exerted by PPh_3 can properly direct metal-donor dissociation. The data collected so far on the reaction of **3** with TPs (thiopurines) always indicated the formation of stable bischelates with a cis,trans arrangement for the N^7,S donor sets and with the *cis*-$Ru(PPh_3)_2$ grouping. A question therefore arose: Can other coordination arrangements for bischelates be obtained from **3**? In principle, the reaction of **3** with a chelating N,S ligand can lead to the formation of the octahedral isomers of the type $Ru(P)_2(N-S)_2$ reported in Scheme 3. Electronic and steric effects discriminate between the possible isomers. From an inspection of molecular models, one would conclude that structure IV is reasonably not favored for TPs; in fact, it is highly hindered because of crashes between H8s from the coplanar bases. In the case of structure V for TP ligands, the two PPh_3 molecules should assume an almost trefoil-shaped arrangement (Scheme 4, Tf-C_3v) instead of a semi-trefoil or tripod-like structure (which would require empty space in the equatorial plane), and such a structure is not favored because of the repulsion between the Ph protons. In the case of the $TPYM^-$ derivatives, structure IV might allow a semi-trefoil arrangement for PPh_3 that would significantly reduce the steric repulsions. Moreover, molecules of types IV and V are predicted to be labile with regard to the dissociation of PPh_3 because of the high trans effect by P. The structures with the *cis*-$Ru(PPh_3)_2$ grouping (I−III) should all be affected by significant steric hindrance from the PPh_3 ligands; the most stable isomer is not easily predictable via inspection of molecular models. From these premises, it appeared important to perform synthetic, experimental, and theoretical structural studies to rationalize the isomerism of bischelation in this class of compounds.

X-ray Crystallography. *cis,cis,trans*-[Ru(PPh$_3$)$_2$(*N,S*-TPYM)$_2$], 1. The coordination sphere around the Ru(II) center for **1** (Figure 1 and Tables 3 and 4) is highly distorted octahedral, and the six donors are the sulfur and nitrogen atoms from the chelating $TPYM^-$ anions and the phosphorus atoms from the PPh_3 molecules (Scheme 3, structure I). The sulfur atoms have a pseudo-trans arrangement found previously for some metal ions chelated by thiopurines (*cis,cis,trans*-$[Ru(PPh_3)_2(N^7,S\text{-HTPR})_2]^{2+}$ and *cis,cis,trans*-$[Ru(PPh_3)_2(N^7,S\text{-H}_2\text{TP})_2]^{2+}$)[7d,7e] or thiopyrimidines (*cis,cis,trans*-

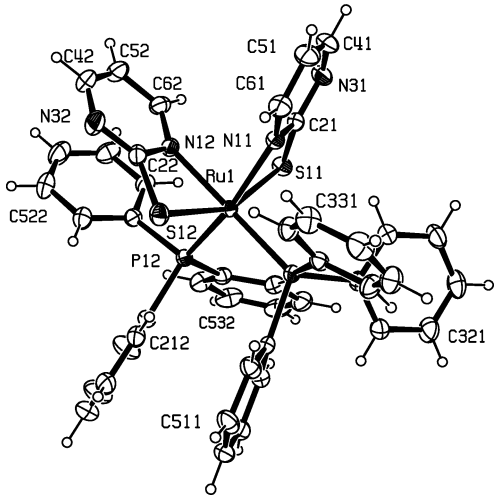

Figure 1. ORTEP-style drawing of *cis,cis,trans*-$[Ru(PPh_3)_2(N,S\text{-TPYM})_2]$ (**1**) with the labeling scheme. Ellipsoids enclose 50% probability.

Scheme 4. Drawing of Possible Conformations for PPh_3 (a) Trefoil C_{3v}, Tf-C_{3v}; (b) Tripod C_{3v}, Tp-C_{3v}; (c) Semi-Trefoil C_s, STf-C_s; (d) Semi-Tripod C_s, STp-C_s; and (e) Semi-Trefoil C_1, STf-C_1

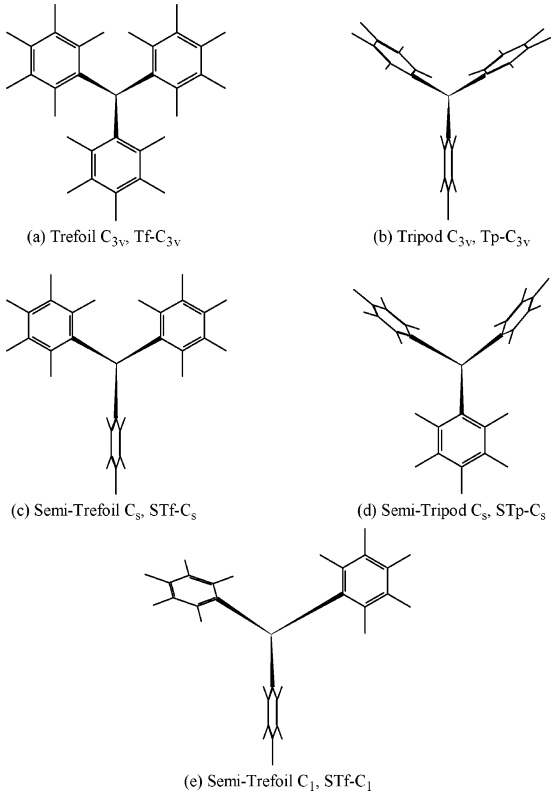

$[Co\{P(OCH_3)_3\}(N,S\text{-TPYM})_2]^+$).[22] It should be noted that the coordination mode VIII (see Scheme 1a) for two $TPYM^-$ ligands toward a Ru(II) center had never been found before. Both the PPh_3 ligands have a semi-trefoil, STf-C_1, type of structure (Scheme 4). The Ru−P bond distances, 2.304(1) and 2.329(1) Å, are in good agreement with the values for *cis,cis,trans*-$[Ru(PPh_3)_2(N^7,S\text{-HTPR})_2]^{2+}$ and are smaller than the value found for the trans isomer (see below). The Ru−S bond distances, 2.388(1) and 2.443(1) Å, are different each other; such a difference was not found in similar molecules

(22) Tong, Y.-X.; Su, C.-Y.; Kang, B.-S.; Yu, X.-L.; Chen, X.-M. *Acta Crystallogr.* **1999**, *C55*, 1800.

Table 3. Selected Bond Lengths (Å) for *cis,cis,trans*-[Ru(PPh$_3$)$_2$(*N*,*S*-TPYM)$_2$] (**1**) and *trans,cis,cis*-[Ru(PPh$_3$)$_2$(*N*,*S*-TPYM)$_2$]·2H$_3$O$^+$·2Cl$^-$ (**2**·2H$_3$O$^+$·2Cl$^-$)

	length	
vector	1	**2**·2H$_3$O$^+$·2Cl$^-$
Ru1−N11	2.167(2)	2.063(3)
Ru1−N12	2.122(2)	
Ru1−P11	2.329(1)	2.369(1)
Ru1−P12	2.304(1)	
Ru1−S11	2.388(1)	2.451(1)
Ru1−S12	2.443(1)	
S11−C21	1.720(3)	1.697(4)
S12−C22	1.724(3)	
N11−C21	1.364(4)	1.356(4)
N12−C22	1.364(4)	
N31−C21	1.339(4)	1.349(4)
N32−C22	1.329(4)	

Table 4. Selected Bond Angles (°) for *cis,cis,trans*-[Ru(PPh$_3$)$_2$(*N*,*S*-TPYM)$_2$] (**1**) and *trans,cis,cis*-[Ru(PPh$_3$)$_2$(*N*,*S*-TPYM)$_2$]·2H$_3$O$^+$·2Cl$^-$ (**2**·2H$_3$O$^+$·2Cl$^-$)

	angle	
vector	**1**	**2**·2H$_3$O$^+$·2Cl$^-$ [a]
N12−Ru1−N11	79.80(9)	
N11−Ru1−N11#1		106.1(1)
N11−Ru1−P12	158.20(6)	
N11−Ru1−P11#1		93.89(8)
N12−Ru1−P12	90.26(7)	
N11−Ru1−P11	93.71(6)	90.91(8)
N12−Ru1−P11	163.75(6)	
P12−Ru1−P11	100.54(3)	
P11#1−Ru1−P11		172.00(4)
N11−Ru1−S11	67.67(7)	67.51(8)
N12−Ru1−S11	91.29(7)	
N11#1−Ru1−S11		172.55(8)
P11−Ru1−S11	100.05(3)	90.13(3)
P12−Ru1−S11	93.45(4)	
P11#1−Ru1−S11		85.82(3)
N11−Ru1−S12	97.00(7)	
N12−Ru1−S12	66.87(7)	
P11−Ru1−S12	99.52(3)	
P12−Ru1−S12	96.82(4)	
S11−Ru1−S12	155.80(3)	
S11−Ru1−S11#1		119.12(4)
C111−P11−Ru1	117.66(8)	115.9(1)
C121−P11−Ru1	120.66(9)	111.4(1)
C131−P11−Ru1	113.05(9)	113.3(1)
C122−P12−Ru1	109.48(9)	
C132−P12−Ru1	115.79(9)	
C112−P12−Ru1	124.1(1)	104.5(2)
C21−S11−Ru1	81.9(1)	78.8(1)
C22−S12−Ru1	81.0(1)	
C61−N11−C21	117.3(3)	119.3(3)
C61−N11−Ru1	141.8(2)	138.4(3)
C21−N11−Ru1	99.2(2)	102.2(2)
C62−N12−C22	117.9(2)	
C62−N12−Ru1	139.2(2)	
C22−N12−Ru1	102.5(2)	
C41−N31−C21	115.3(3)	119.4(3)
C22−N32−C42	115.1(3)	
N31−C21−N11	124.9(3)	120.8(3)
N31−C21−S11	124.6(2)	127.9(3)
N11−C21−S11	110.5(2)	111.3(2)
N32−C22−N12	125.0(3)	
N32−C22−S12	125.6(2)	
N12−C22−S12	109.4(2)	

[a] Symmetry transformation used to generate equivalent atoms for **2**·2H$_3$O$^+$·2Cl$^-$: #1, $-x+1$, y, $-z+3/2$.

for the thiopurine derivatives. Intramolecular interactions might be responsible for the difference (see below). No Ru(II)−S (trans to S) bond for chelating TPYM$^-$ could be found in structures in the CCDB;[6] the Ru(II)−S (trans to P) bond distance is 2.488 Å and was reported for [Ru(TDPME)(*N*,*S*-TPYM)(*S*-TPYM)] [TDPME = 1,1,1-tris(diphenylphosphinomethyl)ethane].[23] The Ru−N bond distances, 2.122(2) and 2.167(2) Å, differ significantly, as well. The Ru−N (trans to P) bond distances for *cis,cis,trans*-[Ru(PPh$_3$)$_2$(*N*^{7},*S*-HTPR)$_2$]$^{2+}$ are in the range 2.10−2.17 Å, whereas the corresponding one for [Ru(TDPME)(*N*,*S*-TPYM)(*S*-TPYM)] is 2.142 Å. The Ru(II)−N (trans to N) bond length for [Ru(BIPY)$_2$(*N*,*S*-TPYM)]$^+$ (BIPY = 2,2′-bipyridine) is 2.104 Å.[24] It should be noted that the shortest Ru−N vector for **1** is trans to the longest Ru−P vector and that the chelate system with the shortest Ru−N bond has the longest Ru−S bond. The latter bond corresponds to the sulfur atom S(12) that has the shortest (C)H···S intramolecular contacts with phenyl ring protons (2.59 and 2.68 Å compared to 2.92 and 2.94 Å). It should be recalled that (C)H···S hydrogen-bond-type interactions were found recently in an unusual thiopurine···thiopurine base pairing.[25] The strain induced by the formation of two four-membered chelate rings and by the vicinity of two bulky *cis*-PPh$_3$ ligands reflects the large deviation from the idealized values (90 and 180°) for the bond angles at metal. The S−Ru−N chelating angles are 67.67(7) and 66.87(7)°. The P−Ru−P and S−Ru−S bond angles are 100.54(3) and 155.80(3)°, respectively. The C2−S bond distances [1.722(3) Å, average] are significantly lengthened with respect to those in the pure thione structures. In fact, the corresponding distance found for the 1,3-dimethyl-2-thio-1,3-pyrimidine cation is 1.630(5) Å.[26] The C2−N1 and C2−N3 bond distances for **1** are 1.364(4) and 1.334(4) Å (average), respectively. The atoms of the TPYM$^-$ anions are almost coplanar, and the S and Ru atoms deviate by 0.0844(4) and 0.3737(4) Å and by −0.0118(4) and 0.1540(4) Å from the N11/C61 and N12/C62 mean planes, respectively. Intramolecular stacking interactions take place between the N12/C62 and C122/C622 rings (shortest contact, N12···C122 = 2.971 Å). It is possible that this interaction has some influence on the Ru−S bond distance (see above). A second type of intramolecular stacking interaction occurs between the C111/C611 and C112/C612 rings (shortest contact, C112···C211 = 3.363 Å). The noncoordinated nitrogen atoms are hydrogen acceptors in a web of C−H···N intermolecular hydrogen-bond-type interactions that involve the phenyl groups and other TPYM$^-$ ligands. For instance, short interactions are N31···C421 ($-x+2$, $-y+1$, $-z+2$) [N···C = 3.639(1) Å, N···H−C = 133(1)°], N31···C532 ($-x+1$, $-y+1$, $-z+2$) [N···C = 3.459(1)Å, N···H−C = 133(1)°], and N32···C42 ($-x+1$, $-y+1$, $-z+1$) [N···C = 3.327(1) Å, N···H−C = 118(1)°]. The existence of this type of interaction for ruthenium−pyrimidine complexes was previously reported and discussed by us in ref 7a.

(23) Landgrafe, C.; Sheldrick, W. S.; Sudfeld, M. *Eur. J. Inorg. Chem.* **1998**, 407.
(24) Yamanari, K.; Nozaki, T.; Fuyuhiro, A.; Kushi, Y.; Kaizaki, S.*J. Chem. Soc., Dalton Trans.* **1996**, 2851.
(25) Cini, R.; Corsini, M.; Cavaglioni, A. *Inorg. Chem.* **2000**, *39*, 5874.
(26) Ferguson, G.; Kaitner, B.; Lloyd, D.; McNab, H.; *J. Chem. Res.* **1984**, *184*, 1760.

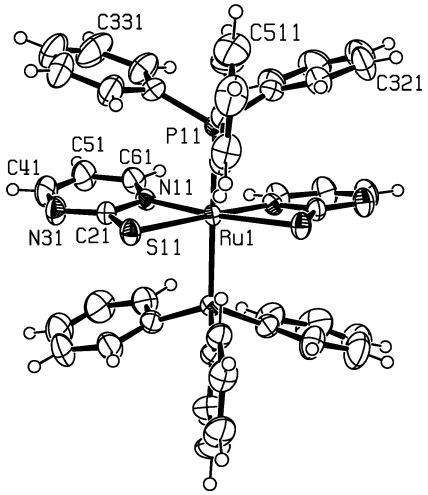

Figure 2. ORTEP-style drawing of *trans,cis,cis*-[$Ru(PPh_3)_2$(*N,S*-TPYM)$_2$] (**2**) with the labeling scheme. Ellipsoids enclose 50% probability. The complex molecule crystallizes with two H_3O^+ molecules and two Cl^- anions (which are not reported in the drawing) per Ru atom. The labels for these particles are O1W and Cl1, respectively.

***trans,cis,cis*-[Ru(PPh$_3$)$_2$(N,S-TPYM)$_2$]·2H$_3$O·2Cl$^-$, 2·2-H$_3$O$^+$·2Cl$^-$.** The coordination sphere for **2** (Figure 2 and Tables 3 and 4) is pseudo-octahedral and consists of two phosphorus atoms (trans to each other) from triphenylphosphine molecules, two sulfur atoms, and two nitrogen atoms from two chelating $TPYM^-$ anions located in the equatorial plane with a head-to-head arrangement (Scheme 3, structure IV). The Ru center is located on a 2-fold crystallographic axis. The Ru−P bond distances are 2.369(1) Å larger than those in **1**, in agreement with a significantly larger trans influence by the P atoms from PPh_3 when compared to N(sp^2) donors (as in the case of **1**). The PPh_3 ligand has an STf-C_s type of structure (Scheme 4). The Ru−S bond distances, 2.451(1) Å, are in agreement with the respective distances found for **1**. The Ru−N bond distances, 2.063(3) Å, are shorter than the Ru(II)−N distances found for **1** and for the thiopurine derivatives because of the lack of the high trans influence from P in the case of **2**. The bond angles at the Ru(II) center deviate significantly from the idealized values of 90 and 180°, because of the formation of the two four-membered coordination rings by the $TPYM^-$. The N−Ru−S (chelating), S−Ru−S, and P−Ru−P angles are, in fact, 67.51(8), 119.12(4), and 172.00(4)°, respectively. It should be noted that equatorial bischelates with $TPYM^-$ ligands have been previously reported for pseudo-octahedral metal complexes and show a wide range for the bond angles at the metal. For instance, *trans,cis,cis*-[Co^{III}{P(Bu^n)$_3$}$_2$(*N,S*-TPYM)$_2$]$^+$ [P(Bu^n)$_3$ = tri-*n*-butylphosphine] has S−Co−S and N−Co−N angles of 106.5 and 108.8°,[27] respectively, and *trans,cis,cis*-[Sn(R)$_2$(*N,S*-TPYM)$_2$] (R, Me or Ph) has S−Sn−S bond angles in the range 85.3−89.9 and N−Sn−N bond angles in the range 149.0−157.6°.[28] The C−S bond [length = 1.697(4)Å] has a greater thione character for **2** than for **1**, in agreement with the weaker Ru−S interaction for **2**. The N3 atom has no linking interaction to the metal but is the hydrogen acceptor for a strong interaction with H_3O^+ (O1W) (x, $-y+1$, $z+0.5$) [N···O = 2.591(6) Å]. The Cl^- anion is also the acceptor of the hydrogen bonds from two H_3O^+ cations: Cl1···O1W (x, y, z) [Cl···O = 3.105(4) Å] and Cl1···O1W ($-x$, y, $-z+0.5$) [Cl···O = 3.017(4) Å]. Intramolecular stacking interactions link the $TPYM^-$ ligand (N11/C61) and two symmetry-related phenyl rings (C131/C631) that sandwich it: C61···C231 = 3.250(6) Å, angle between the planes = 17.56°. No significant intermolecular stacking interactions were revealed.

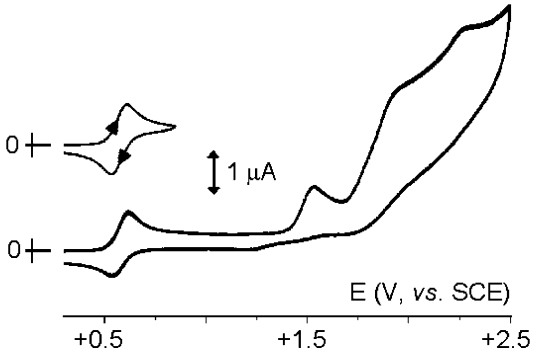

Figure 3. Cyclic voltammetric profiles recorded at a platinum electrode in a CH_2Cl_2 solution of **1** (0.8×10^{-3} M). [NBu_4][PF_6] (0.2 M) supporting electrolyte. Scan rate = 0.2 V s^{-1}.

Table 5. Formal Electrode Potentials (V, vs SCE, 0.246 V vs NHE) and Peak-to-Peak Separations (mV) for the Ru(II)/Ru(III) Oxidation in Different Solvents for the Compounds Investigated in This Work

complex	$E^{\circ\prime}$	ΔE_p[a]	solvent
1	+0.57	74	CH_2Cl_2
	+0.67	59	DMSO
2	+0.51	59	DMSO
3	0.53[b,c]	−	CH_2Cl_2
	0.75[c]	−	DMSO
4	+0.59	123	DMSO
	+0.32	134	H_2O/DMSO (10:1) (buffer, pH 7.4)
5	+0.69	90	DMSO
[$Fe(C_5H_5)_2$]	+0.39	64	CH_2Cl_2
	+0.38	62	DMSO
	+0.24	140	H_2O/DMSO (10:1) (buffer, pH 7.4)

[a] Measured at 0.2 V s^{-1}. [b] From ref 7a. [c] Partial chemical reversibility.

Electrochemistry. Figure 3 illustrates the cyclic voltammetric behavior of **1** in CH_2Cl_2 solution. A first oxidation having features of chemical reversibility ($E^{\circ\prime}$ = +0.57 V, ΔE_p = 74 mV at 0.2 V s^{-1}) precedes a series of irreversible processes (see Table 5). No reduction process was detected in the cathodic window of the solvent (up to −2.1 V). Controlled-potential coulometry in correspondence to the first anodic process (E_w = +0.8 V) consumed one-electron per molecule; thus, we assigned such a step to the $Ru^{II/III}$ process. As a consequence of exhaustive one-electron oxidation, the original yellow solution turned blue, and in confirmation of the complete chemical reversibility of the process, the final solution displayed a voltammetric profile quite complementary to the original one. Indeed, the visible-region spectral pattern accompanying the $Ru^{II/III}$ redox change is illustrated in Figure 4. A band at 640 nm (ϵ, 1120 mol^{-1} cm^{-1} L), which is responsible for the blue color of the oxidized species, is followed by a band at 770 nm (ϵ, 870). The two absorptions can be ascribed to metal-to-ligand charge transfers.[29]

(27) Chen, Z.-N.; Zhang, H.-X.; Kang, B.-S.; Sun, J. *Synth. React. Inorg. Met.-Org. Chem.* **1998**, *28*, 245.
(28) Hadjikakou, S. K.; Demertzis, M. A.; Kubicki, M.; Kovala-Demertzi, D. *Appl. Organomet. Chem.* **2000**, *14*, 727.

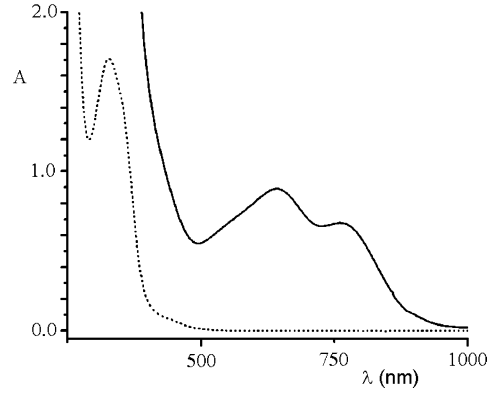

Figure 4. Spectral profiles in the visible region of CH_2Cl_2 solutions of (dashed line) **1** and (solid line) $[\mathbf{1}]^+$. See text.

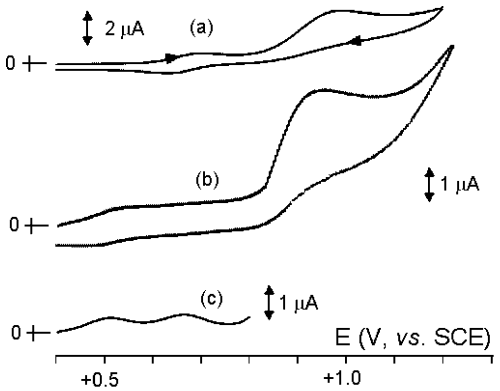

Figure 5. Cyclic voltammetric profiles recorded at a platinum electrode in DMSO solutions of (a) **1** (0.4×10^{-3} M); (b) **2** (0.3×10^{-3} M), scan rate = 0.2 V s^{-1}. (c) Osteryoung square wave voltammogram of the resulting mixture, scan rate = 0.1 V s^{-1}.

Returning to Figure 3, the second irreversible oxidation ($E_p = +1.53$ V) was assigned to the $Ru^{III/IV}$ process, whereas the further oxidations are likely centered on the ligands (for instance, under the same experimental conditions, free PPh_3 oxidizes irreversibly at $E_p = +1.26$ V).[7a]

To enable a comparison of the redox ability of the cis isomer **1** with that of the trans isomer **2**, because of the low solubility of **2** in CH_2Cl_2, the two complexes were examined in DMSO solution where they are slightly soluble (Figure 5). The $Ru^{II/III}$ process for the trans isomer **2** is easier (by 0.16 V) than that of the cis isomer **1,** whereas the $Ru^{III/IV}$ oxidation is superimposed on that of the ligand(s). The more soluble cis complex **4** (in DMSO solution) also affords a chemically reversible $Ru^{II/III}$ oxidation that was found to be slightly easier than that of cis complex **1**. The redox behavior of the complex was also recorded in an aqueous solution (pH 7.4) obtained by a 10-fold dilution with aqueous PBS buffer of a 1×10^{-2} M DMSO solution of **4**. Under these conditions, the $Ru^{II/III}$ oxidation also occurs reversibly. The $Ru^{II/III}$ process for **5** in DMSO solution occurs at potentials close to those for **1**. It should be noted that the redox potentials for **1**, **2**, **4**, and **5** are higher than that previously reported for $Ru^{III/II}$ for the well-known anticancer compound $[RuCl_4(IM)_2]^-$ (IM = imidazole) (−0.386 V, pH 7).[1k,1l]

(29) Nazeeruddin, Md. K.; Zakeeruddin, S. M.; Humphry-Baker, R.; Gorelsky, S. I.: Lever, A. B. P.; Grätzel, M. *Coord. Chem. Rev.* **2000**, *208*, 213.

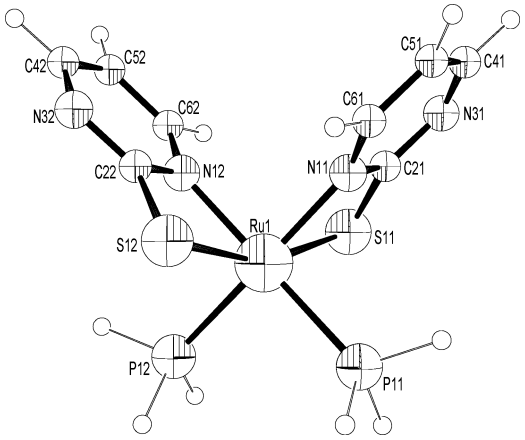

Figure 6. ORTEP-style drawing for *cis,cis,trans*-$[Ru(PH_3)_2(N,S\text{-TPYM})_2]$ (MOD-Jcct, model for **1**) as computed at the DFT-Becke3LYP/BS2 level (see text).

Finally, the precursor *trans*-$[RuCl_2(PPh_3)_3]$, **3**, affords a double-stepped oxidation in DMSO that is reminiscent of the behavior in CH_2Cl_2. Such wave splitting was assigned to the concomitant presence of **3** and $[RuCl_2(PPh_3)_4]$, with the oxidation at lower potentials being attributed to **3**.[7a] Therefore, the replacement of a PPh_3 unit and two Cl^- anions by two chelating N^7,S-TPs or N,S-$TPYMs^-$ ligands stabilizes the $Ru^{II/III}$ couple.

Molecular Modeling Analysis. Density Functional Model. Structures. The structure of $TPYM^-$, deprotonated 2-thio-1,3-pyrimidinate, MOD-E, as optimized at the Becke3LYP/6-31G** level for all atoms, has C2−S and N−C2 bond lengths of 1.719 and 1.382 Å, respectively. On changing the basis set to 6-31G for the C, H, and N atoms but not for sulfur, a small lengthening effect was observed for the N−C2 bonds (by 0.025 Å, 1.8%). A search of the CCDB[6] for the structure of non-metal-bound HTPYM and $TPYM^-$ molecules gave no suggestions, so that a comparative analysis between experiment and calculations could not be performed. The less expensive 6-31G(C,H,N)/6-31G**(S,P)/Lanl2dz-(Ru) basis set (BS2) was considered reliable for the purpose of the present work and used for the simulations of the metal complexes. Selected computed molecules are discussed hereafter. PPh_3 ligands were replaced by PH_3 in the structure of the metal complexes with the aim of decreasing the computational cost. The computed structures of *cis,cis,trans*-$[Ru(PH_3)_2(N,S\text{-TPYM})_2]$ (MOD-Jcct, the model for **1**) and *trans,cis,cis*-$[Ru(PH_3)_2(N,S\text{-TPYM})_2]$ (MOD-Jtcc, the model for **2**) (singlet state, Figures 6 and 7 and Table 6) have Ru−P, Ru−N, and Ru−S bond distances of 2.409, 2.407; 2.089, 2.113; and 2.510, 2.510 Å, respectively. These values compare well with the corresponding ones found in the solid state for **1** and **2** (see above; note that PH_3 replaces PPh_3). The computed P−Ru−P, N−Ru−N, and S−Ru−S bond angles also exhibit good agreement with experiment. Therefore, the DFT methods at the Becke3LYP/BS2 level computed reliable molecular structures for this type of complex.

Energy, Vibrations, and Atomic Charges. The total electronic energy for MOD-Jcct is lower than that for MOD-Jtcc by 3.884 kcal mol^{-1} (ΔE_{el}). It should be noted that the reaction of *trans*-$[RuCl_2(PPh_3)_3]$ with HTPYM

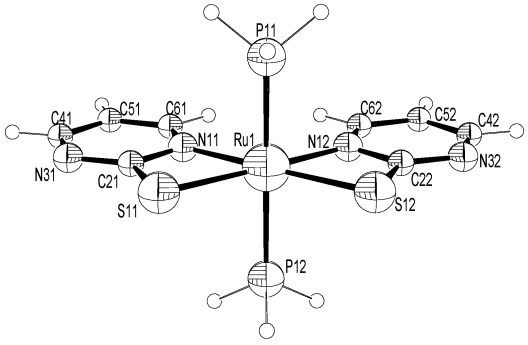

Figure 7. ORTEP-style drawing for *trans*,*cis*,*cis*-[Ru(PH$_3$)$_2$(*N*,*S*-TPYM)$_2$] (MOD-Jtcc, model for **2**) as computed at the DFT-Becke3LYP/BS2 level (see text).

Table 6. Selected Computed Bond Parameters for Molecules *cis*,*cis*,*trans*- and *trans*,*cis*,*cis*-[Ru(PH$_3$)$_2$(*N*,S-TPYM)$_2$] (MOD-Jcct and -Jtcc), Respectively, Optimized at the DFT-Becke3LYP/BS2 Level (See Text)[a]

vectors[a]	MOD-Jcct	MOD-Jtcc
	lengths	
Ru1−S11	2.510	2.510
Ru1−P11	2.409	2.407
Ru1−N11	2.089	2.113
C21−S11	1.736	1.730
C21−N11	1.394	1.404
C21−N31	1.358	1.360
	angles	
S11−Ru1−S12	159.31	114.93
S11−Ru1−P11	89.95	87.50
S11−Ru1−P12	104.44	87.54
S11−Ru1−N11	67.46	67.13
S11−Ru1−N12	97.16	177.94

[a] Numbering scheme similar to that for Figures 6 and 7.

produced the cct isomer, **1**, in higher yield than the tcc isomer, **2**, (ca. 15:1 molar ratio; see above, Experimental Section). A Boltzmann population analysis at 25 °C based on the ΔE_{el} value estimated a MOD-Jcct/MOD-Jtcc molar ratio of 12:1. Even though the agreement between experiment and prediction is good, the analysis should be considered with caution because it did not take into account several factors, including basis set superposition errors, solvent effects, kinetic effects, lattice energies in the solid state, and replacement of PPH$_3$ by Ph$_3$. Molecular modeling analyses carried out via DFT methods have previously been used with success to predict reliable geometrical, spectroscopic, and energetic parameters for similar Ru(II) complexes.[7a,7c]

The analysis of vibrational frequencies for the optimized molecules did not compute any negative frequencies, and the values for selected vibrations for MOD-Jcct are as follows: Ru−N [$\bar{\nu}$ = 671.0 cm^{-1}, k = 315.280 kcal, i(IR) = 5.841 km mol^{-1}], Ru−S (468.9, 223.800, 4.762), C−S (1178.6, 274.918, 37.489), C−N and C−C (1587.5, 979.410, 92.010). On the basis of the computed data, the selected absorption bands found in the spectrum of **1** (see above, experimental) are assigned as follows: 1558 and 1541 cm^{-1}, combined C−C and C−N (TPYM$^-$) stretching vibrations; 1183, C−S vibration; 696, Ru−N vibration. The computed frequencies for MOD-Jtcc have similar values: Ru−N, 665.9 cm^{-1}; Ru−S, 472.5; C−S, 1171.5. Therefore, the analysis of the vibration modes helped in the interpretation of the experimental IR spectra and in the establishment of reliable force fields for MM computations (selected computed atomic charges from the Mulliken population analysis are listed in Table 2). With the aim of finding faster but still reliable computation tools for several complex molecules, approximate quantum mechanics methods were tested.

Semiempirical Model. Structures. The computed structure (ZINDO/1 level) of TPYM$^-$, MOD-E, has C2−S and C2−N bond distances of 1.732 and 1.352 Å, respectively, in good agreement with data computed at the DFT-Becke3LYP/6-31G** level. Bond angles are reproduced well, also. This suggested that the optimizations of HTPYM and TPYM$^-$ ligand molecules, as well as those of Ru−TPYM complexes, be performed at the ZINDO/1 level. The structures of MOD-Fcct (*cis*,*cis*,*trans*-[Ru(NH$_3$)$_2$(PH$_3$)$_2$-(H$_2$S)$_2$]$^{2+}$) and MOD-Gcct molecule (*cis*,*cis*,*trans*-[Ru(NH$_3$)$_2$-(PH$_3$)$_2$(HS)$_2$]) converged nicely (singlet state), and the computed Ru−S and Ru−N bond distances (2.443−2.406 and 2.019−2.017 Å) are in good agreement with the values found for **1**, whereas the computed Ru−P bond distances are larger than those determined experimentally (by ca. 0.2 Å, see below). The optimized MOD-H ([Ru(*N*,*S*-TPYM)]$^+$) structure has Ru−S and Ru−N bond distances of 2.290 and 1.877 Å, respectively, that, as expected, are shorter than the experimental values for **1** and **2** (coordination number of 2 instead of 6). The optimized MOD-Jcct (*cis*,*cis*,*trans*-[Ru-(PH$_3$)$_2$(*N*,*S*-TPYM)$_2$]) structure has Ru−S and Ru−N bond distances of 2.428 and 1.966 Å, respectively. The S−Ru−S and N−Ru−N bond angles are 164.3 and 87.1°, respectively, and compare well with the experimental values for **1** if the difference in the steric hindrance from the PPh$_3$ and PH$_3$ ligands is taken into account. The optimized MOD-Jtcc (*trans*,*cis*,*cis*-[Ru(PH$_3$)$_2$(*N*,*S*-TPYM)$_2$]) structure has Ru−S and Ru−N bond distances of 2.446 and 1.973 Å, respectively, and S−Ru−S and N−Ru−N bond angles of 112.6 and 102.6°, respectively, all of which compare well with the experimental values for **2**. The difference between the computed Ru−P bond distance for MOD-Jtcc and that found for **2** is again significantly large (by ca. 0.15 Å). The computed MOD-Kccc, -Kcct, and -Kttt structures have Ru−S and Ru−N bond lengths in the ranges of 2.445−2.450 Å and 1.990−1.999 Å, respectively. Thus, the Ru−S distances are very well reproduced by theory (largest difference = 0.046 Å), whereas the computed Ru−N lengths are smaller than the experimental values for *cis*,*cis*,*trans*-[Ru-(PPh$_3$)$_2$(*N*^{7},*S*-H$_2$TP)$_2$]$^{+2}$ [7e] and *cis*,*cis*,*trans*-[Ru(PPh$_3$)$_2$(*N*^{7},*S*-HTPR)$_2$]$^{+2}$ [7d] (largest difference = 0.177 Å). The theory/experiment gap for Ru−N can be related to the steric and electronic properties of PPh$_3$ and PH$_3$. In fact, a larger σ-donicity (as well as trans influence) for PPh$_3$ than PH$_3$ is predicted. As noted above for other computed molecules, MOD-K*xxx* have large Ru−P distances (average 2.529 Å) when compared to experiment[7d,7e] (largest difference = 0.173 Å). The lengthening effect of theory on the Ru−PH$_3$ distances must also be related to the donating properties of the two ligands. The influence of the steric hindrance of PPh$_3$ on the conformational space around the Ru−P vectors is analyzed below (see the molecular modeling section).

Table 7. Heats of Formation (ΔH_f^{298}, kcal mol^{-1}) at 25 °C for the Molecules Computed at the ZINDO/1 Level[a]

molecule	ΔH_f^{298}
H^+	353.430
Ru^{2+}	771.173
PH_3 (MOD-A)	−347.530
NH_3 (MOD-A′)	−348.067
H_2S (MOD-A″)	−187.900
HS^- (MOD-A‴)	−42.225
H(S)-HTPYM (MOD-C)	−2134.899
H(N)-HTPYM (MOD-D)	−2163.682
THZ (MOD-D′)	−1464.855
$TPYM^-$ (MOD-E)	−2014.875
H(1),H(9)−H_2TP (MOD-C′)	−2964.934
H(1),H(7)−H_2TP (MOD-C″)	−2965.246
[Ru(*N*,*S*-TPYM)]$^+$ (MOD-H)	−1983.872
trans,*cis*,*cis*-[Ru(NH_3)$_2$(PH_3)$_2$(SH_2)$_2$]$^{2+}$ (MOD-Fctc)	−2000.701
cis,*cis*,*trans*-[Ru(NH_3)$_2$(PH_3)$_2$(SH_2)$_2$]$^{2+}$ (MOD-Fcct)	−2001.435
cis,*trans*,*cis*-[Ru(NH_3)$_2$(PH_3)$_2$(SH)$_2$] (MOD-Gctc)	−2076.181
cis,*cis*,*trans*-[Ru(NH_3)$_2$(PH_3)$_2$(SH)$_2$] (MOD-Gcct)	−2085.968
cis,*cis*,*cis*-[Ru(PH_3)$_2$(*N*,*S*-TPYM)$_2$] (MOD-Jccc)	−5286.369
trans,*cis*,*cis*-[Ru(PH_3)$_2$(*N*,*S*-TPYM)$_2$] (MOD-Jtcc)	−5285.641
cis,*trans*,*cis*-[Ru(PH_3)$_2$(*N*,*S*-TPYM)$_2$] (MOD-Jctc)	−5282.958
cis,*cis*,*trans*-[Ru(PH_3)$_2$(*N*,*S*-TPYM)$_2$] (MOD-Jcct)	−5294.865
trans,*trans*,*trans*-[Ru(PH_3)$_2$(*N*,*S*-TPYM)$_2$] (MOD-Jttt)	−5289.016
cis,*cis*,*cis*-[Ru(PH_3)(*N*^{7},*S*-H_2TP)$_2$]$^{2+}$ (MOD-Kccc)	−6953.199
cis,*cis*,*trans*-[Ru(PH_3)(*N*^{7},*S*-H_2TP)$_2$]$^{2+}$ (MOD-Kcct)	−6958.206
trans,*trans*,*trans*-[Ru(PH_3)(*N*^{7},*S*-H_2TP)$_2$]$^{2+}$ (MOD-Kttt)	−6958.643
cis,*cis*,*trans*-[Ru(PH_3)(*N*-THZ)(*N*,*S*-TPYM)$_2$]$^{2+}$ (MOD-Mcct)	−8120.578
trans,*trans*,*trans*-[Ru(PH_3)(*N*-THZ)(*N*,*S*-TPYM)$_2$]$^{2+}$ (MOD-Mttt)	−8124.001

[a] All Ru(II) species are in their singlet state.

Energy and UV Spectra. A comparative analysis of the heats of formation of the Ru(II) complexes shows that the *cis*,*cis*,*trans*-[Ru(PH_3)$_2$(*N*,*S*-TPYM)$_2$] (MOD-Jcct) molecule (which corresponds to **1**) is more stable than *trans*,*cis*,*cis*-[Ru(PH_3)$_2$(*N*,*S*-TPYM)$_2$] (MOD-Jtcc) (which corresponds to **2**) by 9.224 kcal (Table 7) (this difference is in qualitative agreement with DFT computations; see above). The computed heats of formation for *cis*,*cis*,*trans*- and *trans*,*trans*,*trans*-[Ru(PH_3)$_2$(*N*^{7},*S*-H_2TP)$_2$]$^{2+}$ (MOD-Kcct, −6958.206; MOD-Kttt, −6958.643 kcal) are close, with MOD-Kttt being more stable by just 0.431 kcal. It is reasonable that the differences between the steric and electronic effects of PPh_3 and PH_3 make *cis*,*cis*,*trans*-[Ru(PPh_3)$_2$(*N*^{7},*S*-H_2TP)$_2$]$^{2+}$ the more stable isomer.

The computed electronic spectrum (ZINDO/S) for HTPYM (MOD-C) has selected peaks at 378.9 nm (transition = 5, degeneracy = 1, spin multiplicity = 1, oscillator strength = 0.124) and 285.1 nm (12, 1, 1, 0.363). It should be noted that the computed spectrum for 2-oxo-1,3-pyrimidine (HOPYM) has corresponding bands at 302.5 nm (7, 1, 1, 0.195) and 221.9 nm (12, 1, 1, 0.398). A red shift of ca. 70 nm occurs when a sulfur atom replaces an oxygen atom in pyrimidine or purine bases. The two transitions correspond to charge transfer from the C═S function to the pyrimidine system. The computed values for HTPYM compare well with the spectrum of the pure ligand in DMSO (see above Experimental Section). The peak at 382 nm in the true spectrum is therefore assigned to the transition between HOMO and LUMO, i.e., to transition 5 between MO 18 (−8.0582 eV) and MO 19 (−1.1744 eV) (Figure 8) in the computed spectrum. Therefore, a significant electron transfer from the S atom to the ring occurs once the substance is irradiated at λ = 382 nm. Preliminary computations for the electronic spectrum of [Ru(*N*,*S*-TPYM)]$^+$ (ZINDO/S,[19] singlet) gave a peak at around 400 nm (ligand-to-metal charge transfer), whereas the computed spectrum for $TPYM^-$ has a peak at 348.4 nm (S to ring charge transfer). The metal ligation on $TPYM^-$ causes an increase in the intensity and wavelength for the UV bands close to the visible region (see Experimental Section, molar absorbances for **1** and HTPYM in DMSO). It should be noted that phototherapies on tissues containing thiobase-modified DNA might stem from absorptions in the visible and/or UVA regions[3a] (see below, Conclusion).

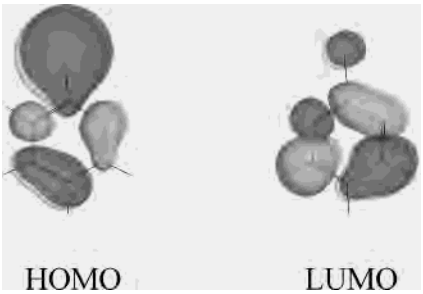

Figure 8. HOMO and LUMO for HTPYM, as computed at the ZINDO/1(S) level. The HOMO−LUMO transition is responsible for the absorption at 382 nm in the spectrum of HTPYM and corresponds mostly to electron transfer from C═S grouping to the pyrimidine ring.

Molecular Mechanics (MM). Structures. The computed bond distances for the optimized structure of *cis*,*cis*,*trans*-[Ru(PPh_3)$_2$(*N*,*S*-TPYM)$_2$] (MOD-Lcct) (Table 8) are in good agreement with experiment (**1**), the largest difference at the coordination sphere being 0.086 Å for Ru−N bonds (computed smaller than experiment). This confirms that the large Ru−N bond lengths found for **1** when compared to **2** are due to the trans influence (that is not taken into account through MM methods) instead of steric effects. The Ru−S bond distances are well reproduced by theory (largest deviations of 0.031 and 0.060 Å). The computed geometrical parameters relevant to the PPh_3 (STf-C_1-type structure, Scheme 4) and $TPYM^-$ moieties are also in agreement with the real molecule. The total strain energy for MOD-Lcct is E_{tot} = 96.35 kcal, and most of the repulsive terms come from electrostatic and steric interactions between PPh_3 ligands. The analysis of the conformational space for the cis,cis,-trans structure performed by rotating the PPh_3 unit around the Ru−P bond revealed another minimum-energy structure (E_{tot} = 95.86 kcal, barrier between the two minima = 4.5 kcal). The optimized structure of *trans*,*cis*,*cis*-[Ru(PPh_3)$_2$(*N*,*S*-TPYM)$_2$] (MOD-Ltcc, E_{tot} = 97.15 kcal) is similar to the X-ray structure for **2** (RMS deviation for the coordination-sphere atoms = 0.088 Å) and has Ru−P, Ru−N and Ru−S bond distances of 2.377 (average), 2.071, and 2.419 Å, respectively, in agreement with the found values. The total strain energy for the optimized structure of *trans*,*trans*,*trans*-[Ru(PPh_3)$_2$(*N*,*S*-TPYM)$_2$] (MOD-Lttt) is 98.67 kcal. The (Ph)H···S contact distances computed for MOD-Ltcc are ca. 2.98 Å [van der Waals radii, H = 1.2, S = 1.8 Å;

Table 8. Selected Bond Lengths (Å) and Angles (°) for the Selected Molecules Optimized via MM Methods by Using the ad Hoc Amber-type Force Fields (Table 2): HTPYM (MOD-C), $TPYM^-$ (MOD-E), *cis*,*cis*,*trans*-, *trans*,*cis*,*cis*-, and *trans*,*trans*,*trans*-[$Ru(PPh_3)_2$(*N*,*S*-TPYM)$_2$] (MOD-Lcct, -Ltcc, -Lttt)[a]

	molecules				
vectors	MOD-C	MOD-E	MOD-Lcct	MOD-Ltcc	MOD-Lttt
			lengths		
Ru1−N11			2.081	2.070	2.076
Ru1−N12			2.069	2.073	2.072
Ru1−P11			2.383	2.379	2.373
Ru1−P12			2.372	2.375	2.381
Ru1−S11			2.419	2.417	2.414
Ru1−S12			2.419	2.421	2.421
N11−C21	1.353	1.338	1.317	1.319	1.321
C21−S11	1.611	1.750	1.690	1.695	1.693
C21−N31	1.341	1.338	1.334	1.333	1.333
			angles		
N11−Ru1−N12			79.62	113.48	177.80
N11−Ru1−P11			96.87	89.56	92.36
N11−Ru1−P12			157.13	91.47	86.53
N11−Ru1−S11			64.43	64.88	64.94
N11−Ru1−S12			103.46	176.01	117.59
N12−Ru1−P11			160.95	96.03	88.59
N12−Ru1−P12			91.62	88.62	92.45
N12−Ru1−S11			101.28	175.32	113.15
N12−Ru1−S12			64.62	64.44	64.42
P11−Ru1−P12			97.94	174.40	177.69
P11−Ru1−S11			93.86	88.38	87.10
P11−Ru1−S12			98.55	87.32	87.46
P12−Ru1−S11			97.22	87.06	90.59
P12−Ru1−S12			91.45	91.88	94.85
S11−Ru1−S12			163.75	117.48	174.11
N11−C21−S11	117.8	119.5	106.27	106.44	106.62
N31−C21−S11	117.9	119.5	129.78	129.95	129.62
N11−C21−N31	124.3	121.1	123.61	115.84	123.76
C21−N31−C41	117.0	118.5	116.27	123.61	115.82
C61−N11−C21	120.0	119.2	118.69	120.09	119.86

[a] Numbering scheme similar to that for Figure 1.

computed atomic charges (DFT), H(Ph) = 0.159 e, S = 0.063], whereas the (Ph)H···H contact distances are 2.785 and 2.333 Å [charge on H^6(TPYM) = 0.225 e]. Therefore, it is reasonable that the steric and electrostatic repulsions between the H atoms discriminate between the trans,trans,-trans and trans,cis,cis configurations and favor the latter.

Biology. Spectrophotometric Analysis of the Solution Behavior. The solution behavior of *cis*,*cis*,*trans*-[$Ru(PPh_3)_2$(*N*,*S*-TPYM)$_2$] (**1**), *cis*,*cis*,*trans*-[$Ru(PPh_3)$(*N*-THZ)(N^7,*S*-H_2TP)$_2$]Cl_2 (**4**), and *cis*,*cis*,*trans*-[$Ru(PPh_3)_2$(N^7,*S*-HTPR)$_2$]Cl_2 (**5**) was analyzed spectrophotometrically in some more detail so that the reactivities of the complexes with biomolecules could be evaluated. All of the compounds are poorly soluble in aqueous media but are soluble in DMSO. Thus, concentrated DMSO solutions of all of the compounds (1×10^{-2} M) were prepared. They exhibit a relatively high stability; indeed, no appreciable spectral changes were observed over 24 h of monitoring at 25 °C. The stability of the solutions was further assessed under physiological-like conditions. For this purpose, the concentrated DMSO solutions were diluted to 1×10^{-4} M with standard phosphate buffer containing NaH_2PO_4 (50 mM) and NaCl (100 mM) at pH 7.4. Notably, **1** and **5** are appreciably stable, whereas **4** exhibited evidence of time-dependent spectral changes (Figure 9).

Interactions with Bovine Serum Albumin (BSA). To further elucidate the reactivity of the selected metal complexes with potential biomolecular targets, their interactions with BSA were assayed through a simple protocol.[30] Such a protocol consists of a series of time-dependent spectrophotometric analyses coupled to ultrafiltration experiments. Reliable results were obtained only for **4**; in contrast, **1** and **5** underwent extensive precipitation in the course of the experiments. Fresh, buffered solutions of **4** were prepared as reported above, and a stoichiometric amount of BSA was promptly added. The resulting mixture was incubated at 25 °C for 24 h, monitored spectrophotometrically, and then subjected to ultrafiltration. The upper and lower solutions were analyzed spectrophotometrically. After a series of ultrafiltration cycles, the amount of protein-bound ruthenium was reduced to 50% of the original value. This finding suggests that the interactions of BSA with **4** are tight and reversible, i.e., noncovalent in nature.

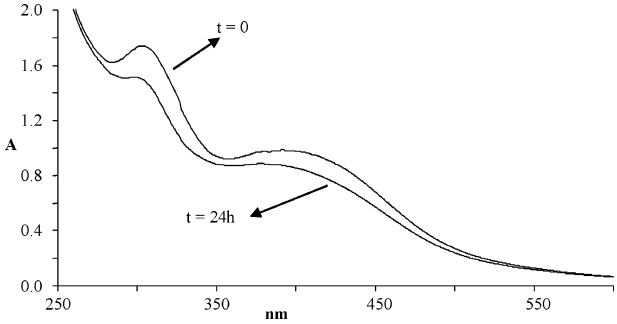

Figure 9. Electronic spectra of *cis*,*cis*,*trans*-[$Ru(PPh_3)$(*N*-THZ)(N^7,*S*-H_2-TP)$_2$]Cl_2 (1×10^{-4} M) in phosphate buffer pH 7.4.

Table 9. Inhibitory Effects of *cis*,*cis*,*trans*-[$Ru(PPh_3)$(*N*-THZ)(N^7,*S*-H_2TP)$_2$]Cl_2 (**4**) and *cis*,*cis*,*trans*-[$Ru(PPh_3)_2$(N^7,*S*-HTPR)$_2$]Cl_2 (**5**) on the Growth of Cisplatin-Sensitive Ovarian Carcinoma A2780/S Human Cell Line, Expressed as IC_{50} (μM)[a]

compound	IC_{50}
4	17 ± 1
5	29 ± 9
cis-[$Pt(NH_3)_2${*O*,*O*′-$COO)_2CCH_2CH_2CH_2$(C)}], carboplatin	6.0 ± 0.7[31]
cis-[$PtCl_2(NH_3)_2$], cisplatin	0.50 ± 0.18

[a] Values for A2780/R, HT29, MCF7, and A549 cell lines give IC_{50} > 100 μM for both **4** and **5**.

Interactions with Calf Thymus DNA. The interaction of **4** with calf thymus DNA was analyzed through an experimental protocol analogous to that used for BSA. Remarkably, in contrast to the case of the BSA, no significant interaction between **4** and DNA could be revealed.

Cytotoxic Activity. Compounds **4** and **5** have the potential to produce inhibitory effects on fast-growing cancer cell lines and to be good candidates as anticancer drugs. With this in mind, the cytotoxic effects of these complexes against five tumor cell lines were tested (see above, Experimental Section). Concentrations ranging from 5 to 100 μM of each compound were used. Some significant cytotoxic effects were observed toward the A2780/S cell line as reported in Table 9, even though they were lower than those found for classical platinum drugs. The IC_{50} values for the A2780/R, HT29,

(30) Messori, L.; Orioli, P.; Vullo, D.; Alessio, E.; Iengo, E. *Eur. J. Biochem.* **2000**, *267*, 1206.

Scheme 5. Possible Reaction Pathways to Produce Different $[Ru(P)_2(N-S)_2]$ Isomers from *trans*-$[RuCl_2(PPh_3)_3]$

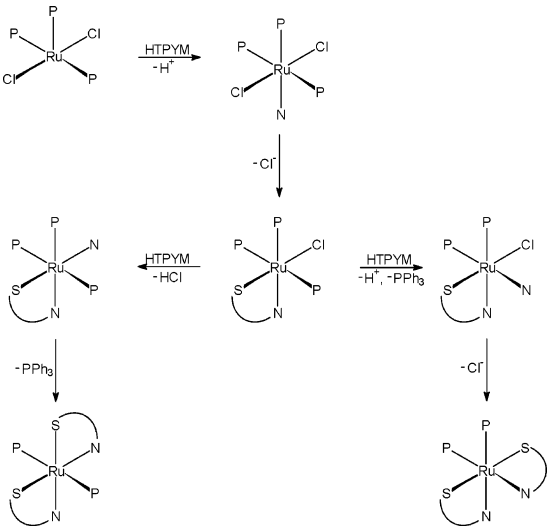

MCF7, and A549 cell lines exceeded the maximum tested concentration of 100 μM and are not reported.

Conclusion

Reactivity. The routes for the synthesis of new ruthenium(II)−thiopyrimidine complexes have been presented. The thiobase acts as a chelating ligand, and the formation of a bischelate is favored at least for ligand/metal molar ratios close to 2:1, even though the coordination rings are highly strained. Of the five possible $[Ru(P)_2(N-S)_2]$ bischelates (Scheme 3), only two (cis,cis,trans and trans,cis,cis) for thiopyrimidine and one (cis,cis,trans) for thiopurines have been found and isolated, at least from *trans*-$[RuCl_2(PPh_3)_3]$, **3**, in alcoholic media.

A gross sequence of reactions for the formation of *cis*,*cis*,*trans*- and *trans*,*cis*,*cis*-$[Ru(P)_2(N-S)_2]$ from **3** and thiopyrimidines or thiopurines is tentatively depicted in Scheme 5, although different routes cannot be ruled out.

Molecular modeling analysis has shown that the cis,cis,-trans isomers are more stable than the trans,cis,cis ones. The two PPh_3 ligands significantly influence the nature and geometry of the bischelates.

cis,*cis*,*trans*-$[Ru(P)_2(TPs)_2]$ isomers can be described as head-to-tail, HT, as regards the relative orientation of the two purines. It should be noted that this type of configurations is common for $Pt(purine)_2$ complexes.[32] Nevertheless, other isomers might become favored if PPh_3 is replaced by a less space-demanding ligand.

Cis,cis,trans isomers can be reversibly oxidized to $[Ru^{III}(P)_2(N-S)_2]^{+/3+}$ (electrochemistry) at potentials (ca. 0.50 V vs SCE) accessible through several common oxidizing agents. However, the species $[Ru^{II}(P)_2(N-S)_2]^{0/2+}$ are favored in hypoxic environments such as tumoral tissues.

The search into water-soluble ruthenium−thiobase complexes suitable for the formation of adducts with proteins and nucleic acids required that the number of PPh_3 ligands per Ru center be decreased or the hydrophilicity of the thiobase be increased. This objective was in part reached (see also ref 7c) by using a specific synthetic route from **3** to *trans*-$[RuCl_2(PPh_3)(N\text{-THZ})_3]$ to *cis*,*cis*,*trans*-$[Ru(PPh_3)(N\text{-THZ})(N^7,S\text{-}H_2TP)_2]Cl_2$ (**4**) or by using thiobase nucleosides (that have several peripheral hydrophilic OH groups).

Spectroscopy. This work has shown that the C═S group is a useful probe for light and a diagnostic for thiobases and their metal compounds. DFT calculations helped to interpret the overall infrared spectra of ruthenium−thiobase complexes and to show that vibrations of the metal-bound thione functions absorb at ca. 1180 cm^{-1} (1183 for **1**).

UVA/vis light interacts with thiobases more than with typical nucleobases because of the presence of C═S groupings. Experimental and theoretical results showed that charge transfers from C═S to ring atoms or to the Ru center are responsible for the absorptions in the regions for free ligands and metal-bound bases, respectively. Further work on absorption and fluorescence spectroscopy in the UV/vis region for ruthenium−thiobase complexes, as well as for Ru-*S*-DNA/RNA, is worthy of additional effort, especially in relation to PDTs.[3a]

Biology. The present work has shown that at least two ruthenium(II)−thiopurine complexes have significant cytotoxic activities toward ovarian human tumor cell lines. The rationale for this activity might come from the effect of the ligand once dissociation of the ruthenium−thiobase linkages occurs inside the cell, as well as from the subsequent attack of the metal residue on biomolecules. The incorporation of thiopurines into nucleic acids is reported to be a key step in the mechanism for the anticancer activity of those drugs (see ref 3a and references therein).

The present work shows that thiobase-containing nucleic acids should be very reactive toward Ru(II) centers and that the $Ru^{II,III}$-*S*-DNA/RNA adducts are strong UVA/vis absorbers. These observations suggest that thiobases (as light sensitizers) be inserted into the DNA/RNA of tumoral tissue and chemotherapic Ru-based treatments and phototherapic applications be applied, especially against superficial malignancies.

The cytotoxic activity for the thiopyrimidine complex **1** could not be determined owing to its insolubility in water. However, in vivo anticancer and antimetastatic tests for **1**, **2**, **4**, and **5**, as well as analogous derivatives, are worthy of further investigation.

Preliminary MM analyses (Amber-type force field; water as solvent) were performed on single-strand and double-strand B-conformation trinucleotides of the type ApXpAp (X = T, G, C for DNA and U, G, C for RNA). As expected, the effect of the substitution of sulfur for oxygen in position 6 for G and position 4 for T and U on the conformation of single-strand molecules is small. Larger changes occur for double-strand DNA because of the significant weakening for the base pairing.[33] This change makes the S donor or the N−S chelator more accessible to an eventual metal center coming from the major grove. The chelation of metal ions from N^7,*S*-thiopurine−DNA should be preferred over che-

(31) Aird, R. E.; Cummings, J.; Ritchie A. A.; Muir M.; Morris R. E.; Chen H.; Sadler P. J.; Jodrell D. I. *Br. J. Cancer* **2002**, *86*, 1652.
(32) Barnham, K. J.; Bauer, C. J.; Djuran, M. J.; Mazid, M. A.; Rau, T.; Sadler, P. J. *Inorg. Chem.* **1995**, *34*, 2826.

lation via *N*,*S*-thiopyrimidine−DNA owing to the higher stability of five-membered chelation rings than four-membered ones and to the easier structural accessibility of thiopurines with respect to thiopyrimidines in the double-strand DNA molecule. 2-thiocytosine−DNA is not easily accessed from incoming metal centers, when compared to 4-thiothymine and 4-thiouracil. The metal chelation of a $RuCl_4$ center from N^7,*S*-thioguanine of a double-strand B-DNA trinucleotide ApGSpAp causes severe structural changes (see ESI section).

Acknowledgment. The authors gratefully acknowledge Professor E. Mini (Laboratorio di Chemioterapia, Dipartimento di Farmacologia Preclinica e Clinica, University of Florence, Florence, Italy) for the cell culture and for allowing G.M. to perform cytotoxic experiment at his laboratory. Professor M. Gregorkiewitz (Dipartimento di Scienze della Terra, University of Siena, Siena, Italy) is gratefully acknowledged for the EDAX-SEM analyses. Mr. F. Berrettini (CIADS, Centro Interdipartimentale di Analisi e Determinazioni Strutturali, University of Siena) is acknowledged for the X-ray data collection. R.C. acknowledges University of Siena for funding. P.Z. gratefully acknowledges the financial support from CNR (Consiglio Nazionale delle Ricerche, Roma, Italy, Agenzia2000 CNR00AAFB). CIRCMSB (Consorzio Interuniversitario per la Ricerca nella Chimica dei Metalli nei Sistemi Biologici, Bari, Italy) is gratefully acknowledged for a grant to G.T. CINECA (Consorzio Interuniversitario per il Calcolo Automatico dell'Italia Nord-Orientale, Casalecchio di Reno, Bologna, Italy) is acknowledged for Grant 2002/2003-0306.

Supporting Information Available: Tables of atomic coordinates, bond lengths, and angles for structures computed via DFT (12S−18S), semiempirical (19S−72S), and MM (73S−91S) methods. Table 92S of the heat of reaction as computed from the heat of formation of selected molecules optimized at the ZINDO/1 level. Tables of X -ray crystal data, atomic coordinates, bond lengths and angles, anisotropic displacement parameters for all non-hydrogen atoms, and hydrogen atom coordinates with isotropic displacement parameters (1S−11S). X-ray crystallographic file in CIF format (CCDB numbers 219524 and 219525). Figures of optimized structures for MOD-E (DFT: MOD-A, -A′, -A″, -A‴, -B, -C, -C′, -C″, -D, -D′, -E, -Fctc, -Fcct, -Gctc, -Gcct, -H, -Icct, -Jccc, -Jtcc, -Jctc, -Jcct, -Jttt, Kccc, -Kcct, -Kttt, -Mcct, -Mttt. ZINZO/1: MOD-B, -C, -E, -Lcct, -Ltcc, -Lttt, -Ncct, -Nttt, -ApGpAp, -ApGSpAp, -ApGSpApRuCl4. This material is available free of charge via the Internet http://pubs.acs.org.

IC0349095

(33) Basilio Janke, E. M.; Dunger, A.; Limbach, H. H.; Weisz, K. *Magn. Reson. Chem.* **2001**, *39*, 5177.